photonics

MDPI

Review

Conformational Dynamics of Biopolymers in the Course of Their Interaction: Multifaceted Approaches to the Analysis by the Stopped-Flow Technique with Fluorescence Detection

Nikita A. Kuznetsov [1,2]

[1] Institute of Chemical Biology and Fundamental Medicine, Siberian Branch of Russian Academy of Sciences, Novosibirsk 630090, Russia; nikita.kuznetsov@niboch.nsc.ru
[2] Department of Natural Sciences, Novosibirsk State University, Novosibirsk 630090, Russia

Abstract: This review deals with modern approaches to systematic research on molecular-kinetic mechanisms of damage recognition and removal by pro- and eukaryotic enzymes of DNA base excision repair. To this end, using DNA glycosylases from different structural families as an example—as well as apurinic/apyrimidinic endonuclease, which differs structurally and catalytically from DNA glycosylases—a comprehensive methodology is described in detail regarding studies on the mechanisms of action of DNA repair enzymes in humans and in *Escherichia coli*. This methodology is based on kinetic, thermodynamic, and mutational analyses of alterations in the conformation of molecules of an enzyme and of DNA during their interaction in real time. The described techniques can be used to analyze any protein–protein or protein–nucleic acid interactions.

Keywords: enzymatic activity; mechanism; catalysis; pre-steady-state kinetics; thermodynamics; mutational analysis; fluorescence; DNA damage; base excision repair; DNA glycosylase; AP endonuclease

Citation: Kuznetsov, N.A. Conformational Dynamics of Biopolymers in the Course of Their Interaction: Multifaceted Approaches to the Analysis by the Stopped-Flow Technique with Fluorescence Detection. *Photonics* **2023**, *10*, 1033. https://doi.org/10.3390/photonics10091033

Received: 20 July 2023
Revised: 30 August 2023
Accepted: 6 September 2023
Published: 8 September 2023

1. Introduction

The ability of proteins and nucleic acids to exist in different conformations is a unique feature of biopolymers. Enzymatic processes involving these macromolecules, including stages of substrate binding and catalytic reactions, are also accompanied by conformational rearrangements. There is a direct relationship between the conformational dynamics of interacting molecules and the functional activity and efficiency of enzymes.

Currently, the understanding of mechanisms underlying enzymatic reactions is mostly based on static structural data from X-ray diffraction analysis and NMR spectroscopy, steady-state kinetic data (which allow to compare the specificity of an enzyme for various substrates and rates of their conversion), and structural analysis of the intermediates and substrate conversion products.

Undoubtedly, structural-analysis techniques make a large contribution to the elucidation of the nature of enzymatic catalysis, but they can provide information only about a certain fixed state of an enzyme and substrate at a certain time point in an enzymatic process, for example, within a catalytic complex. After the set of processes that must occur for the formation of a catalytic complex is determined by structural analyses, the sequence of these events remains completely unclear, as do the nature of the interactions at the initial stages of substrate recognition, the nature of the stages that ensure enzyme specificity, and the effective discrimination of the substrate from a "nonsubstrate".

To answer these questions and understand the mechanisms of a specific enzyme–substrate interaction, it is necessary to analyze conformational dynamics in the course of the interaction. A substantial contribution to the understanding of the mechanisms behind a specific enzyme–substrate interaction is made by studies on the pre-steady-state kinetics and

thermodynamics of an enzymatic process with the registration of conformational transformations of the interacting molecules. Thus, the analysis of conformational dynamics, which is an integral part of all approaches to the investigation of the mechanism of an enzyme's action, is an important and relevant field of modern research.

Enzymes of the base excision DNA repair system, namely DNA glycosylases and apurinic/apyrimidinic (AP) endonucleases, have been used as examples of studying conformational dynamics in processes of specific recognition of a substrate. It is known that cellular DNA, in the course of its functioning, is constantly exposed to various factors that can cause damage. Oxidation, alkylation, deamination, hydrolysis of *N*-glycosidic bonds, formation of breaks in the sugar-phosphate backbone, and cross-linking of DNA strands are only a few of the processes leading to DNA lesions. To counteract the accumulation of damage in DNA, every living organism has a specialized system for protecting DNA from damage: the DNA repair system. There are five fundamental pathways responsible for the repair of damaged DNA: nucleotide excision repair, base excision repair, correction of mismatched DNA bases, DNA repair during homologous recombination, and nonhomologous recombination during joining DNA ends [1]. The base excision repair (BER) pathway is one of the major pathways counteracting the genotoxic effects of nonbulky DNA lesions frequently arising in the cellular genome [2–6]. The BER pathway is a multistep process that can be reconstituted using a limited number of proteins, including a damage-specific DNA glycosylase, AP endonuclease, DNA polymerase, and DNA ligase [7–9]. The results of studies [10–15] suggest that DNA repair plays an important role in the development of cancer. Today, it is still relevant to study the full functioning of DNA repair pathways as well as the relationship between failures in these mechanisms and an increased risk of developing certain diseases [16,17]. Taken together, enzymes of the repair system play an important role in the maintenance of DNA integrity and perform a crucial function in the physiology of any organism; therefore, they are a relevant subject of research.

2. General Principles of Investigation into Conformational Dynamics in Real Time

The analysis of the conformational mobility of the structure of an enzyme and a substrate during their interaction is a difficult and nontrivial task that requires a wide range of research methods and diverse approaches. It is interesting to reflect upon the perceived popularity of fast kinetic techniques and their functional evolution with time. In the 1920s, the so-called "flow method" was developed, which allows one to monitor the course of reactions that take place in hundredths of a second. The essence of flow methods is that the reaction is initiated by the fast mixing of the reagents under flow conditions. It should be noted that initially, flow methods have significant limitations in terms of detection type, model system availability, volumes of reactants and their concentrations, lack of mathematical apparatus for computational analysis of the kinetic traces, etc. However, over the years, these mixing methods, especially the stopped-flow variant, were improved by minimization of reactant concentration owing to an increase in the sensitivity of fluorescence detection. Progress in the technology of purification of any target enzyme in the required quantities using laboratory cell-producers and designed expression vectors, the possibility of creating chemically complex synthetic substrates and ligands, the creation of new bright and microenvironmentally sensitive fluorescent dyes, as well as many other achievements of modern molecular biology, led to the development of fast kinetic techniques up to the highest level in the field of understanding the molecular mechanisms of the enzyme's action.

Fluorescence spectroscopy is widely used to study enzyme–substrate interactions [18,19]. Conformational transformations of proteins have been registered by means of changes in their intrinsic fluorescence from tryptophan residues. Tryptophan is the most fluorescent amino acid, and approximately 90% of all protein fluorescence is typically due to its presence. Another fluorescent amino acid, tyrosine, contributes to the emission spectrum only when it is found in large excess over tryptophan in the protein under study. Tryptophan fluorescence is very sensitive to the polarity of its environment and is quenched

by various molecules, including DNA. The spectral maxima of a protein's fluorescence emission depend on the immediate environment of tryptophan residues in the polypeptide molecule. For instance, a shift to a shorter-wavelength region is interpreted as a consequence of the shielding of tryptophan residues from the aqueous phase. On the other hand, denaturation causes a shift to a longer wavelength in the fluorescence emission spectrum and approximately the same maximum in the emission spectra of all proteins. The position of a maximum in a fluorescence spectrum changes if tryptophan residues participate in an interaction, and this effect makes it possible to monitor the process of DNA–protein binding [20–22]. Nonetheless, one must keep in mind that most proteins contain several Trp residues with different environments, and therefore the spectral properties of these residues may differ. Accordingly, the data obtained by registration of changes in fluorescence intensity of Trp residues, in the general case, enable an investigator to draw a conclusion about the overall conformational dynamics of an enzyme.

Conformational transitions in nucleic acids can be detected using fluorescent analogs of heterocyclic bases (Figure 1a) [23–28]. The fluorescence of most of these analogs is quenched by neighboring bases, and the efficiency of this quenching depends on the nature of the neighboring bases and on the DNA conformation. 2-Aminopurine (aPu) has found the largest number of applications in the research field of enzyme–substrate interactions [20,21,29–33]. Compared with free aPu, the fluorescence intensity of aPu within DNA is lower due to stacking with adjacent bases. Aside from aPu, cytosine analogs are also widely used, for example, pyrrolocytosine (C^{Py}) [34–37] and 1,3-diaza-2-oxophenoxazine (tC^{O}) [38–44]. C^{Py} fluorescence is quenched within a double-stranded DNA structure as compared with a single-stranded structure [45,46]. Additionally, a set of new fluorophores have been employed and tested, for example, naphtho [1,2,3-cd]indol-6(2*H*)-one [47] and 3-hydroxychromone [35,48–50]. Thus, the use of substrates containing fluorescent analogs of nitrogenous bases helps to register conformational changes in DNA substrates during the assembly of an enzyme–substrate complex.

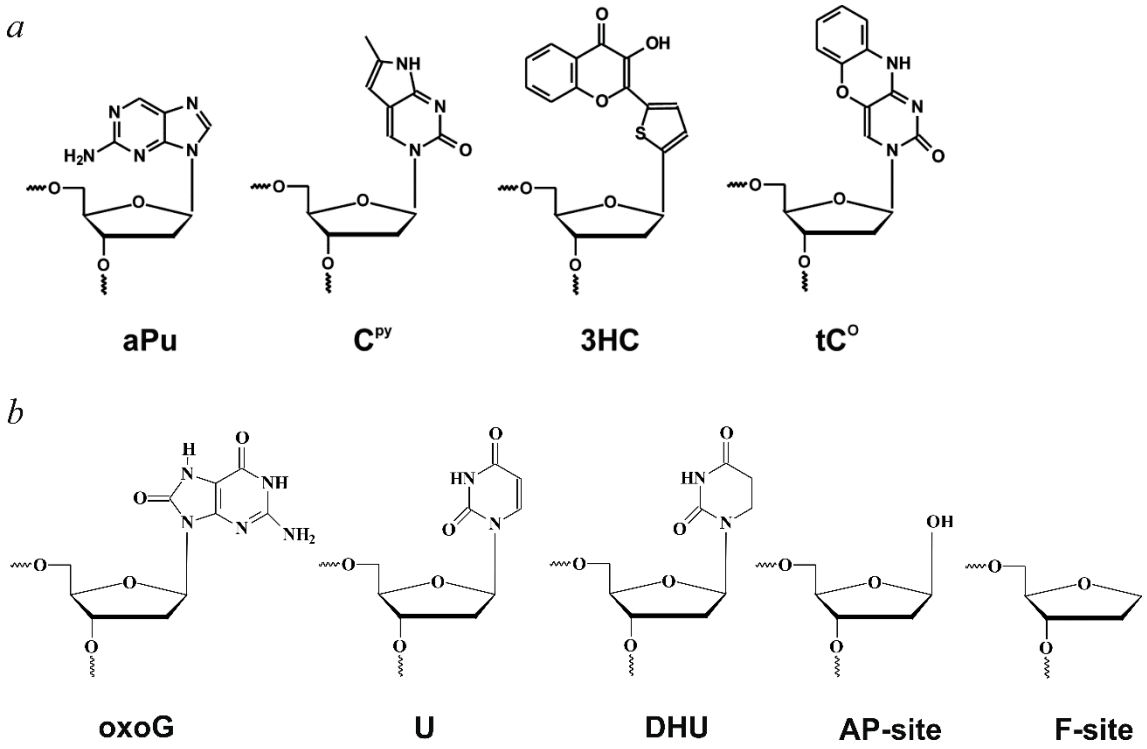

Figure 1. Structures of the nucleotides used in the reviewed studies. (**a**) Fluorescent analogs of nitrogenous bases; (**b**) damaged nucleotides and uridine, which are specifically recognized by enzymes described in the present review.

Another way to study conformational transitions in DNA that we have used in our research is the fluorescence resonance energy transfer (FRET) method, which makes it possible to record changes in the distance between fluorescence donor and acceptor residues located in different parts of a biomolecule [51–56]. In this context, pairs of fluorescent dyes can be located at (1) different ends (labelled by 5′ sides of complementary strands) or (2) on one side (labelled by 5′ and 3′ sides of complementary strands) of a DNA substrate, thereby enabling effective registration of processes that lead to a change in the distance between the dyes. Furthermore, the former approach makes it possible to efficiently record DNA bending during the formation of a complex with the enzyme, whereas the latter arrangement of dyes is more sensitive to the catalytic stage and subsequent dissociation of the enzyme–product complex, and this process extends the distance between the fluorescence donor and acceptor.

An integral part of kinetic research with fluorescent detection has been the choice of the most sensitive model system of DNA substrates, in which a fluorescent group can be located on the 5′ or 3′ side of a lesion or in the complementary strand opposite the damage. For each enzyme, a comparative analysis of such model substrates should be performed, which will allow us to choose the type of system that has the highest sensitivity to conformational changes in DNA.

In the present review, as an example of multifaceted approaches to the analysis of biopolymer conformational dynamics by the stopped-flow technique with fluorescence detection, the set of pro- and eukaryotic enzymes involved in DNA base excision repair was described. To characterize various stages of an enzymatic process, the method of a stepwise increase in ligand complexity has been employed [57]. A DNA substrate is defined as a DNA duplex that, after binding to the active site of an enzyme, undergoes chemical transformations. A DNA ligand is a DNA duplex that can bind within the active site of an enzyme but does not undergo chemical transformation. The structures of all modified nucleotides are given in Figure 1b. A duplex containing a damaged nucleotide in one of the strands has been used as a specific substrate, thus ensuring the formation of all possible contacts and specific bonds between the enzyme and damaged DNA. In the case of DNA glycosylases, oligonucleotides carrying a damaged base, such as 8-oxoguanine (oxoG), 5,6-dihydrouracil (DHU), or uracil (U), have been chosen as specific substrates. For AP endonucleases, such substrates are duplexes carrying an AP-site or its 2-oxymethyl-3-oxy-tetrahydrofuran analog (an F-site). For DNA glycosylases, duplexes containing an AP-site, which is an intermediate product of the reaction, have served as a simplified model of interaction with a substrate where there are no stages of specific recognition of the damaged base. The use of a nonreactive analog of an AP-site containing a 2-oxymethyl-3-oxy-tetrahydrofuran residue (an F-site) instead of 2′-deoxyribose allows us to characterize only the stages of binding of a DNA glycosylase to damaged DNA. The duplex carrying an F-site has all the specific features of the AP-site but is resistant to incision by DNA glycosylases because it does not contain a hydroxyl group at the 1′ position. Duplexes of oligonucleotides containing no modified nucleosides have been used as nonspecific substrates.

Comparison of a model system involving a nonspecific DNA duplex (the simplest nonspecific interactions) with a model system involving a duplex containing an F-site (specific binding, an analog of a DNA glycosylase product, or a substrate for AP endonucleases) or an AP-site (specific binding, a β-elimination reaction catalyzed by some DNA glycosylases, or phosphodiester bond hydrolysis catalyzed by AP endonucleases), and then with a model system involving a specific DNA substrate containing a damaged base (the full enzymatic reaction cycle catalyzed by DNA glycosylases), allowed to reveal additional interactions between the reacting molecules and, as a consequence, additional conformational changes in both the enzyme molecule and the substrate molecule. This approach makes it possible to correlate conformational alterations in biopolymers with interactions of certain residues during the assembly of a specific enzyme–substrate complex.

Because the recognition and conversion of substrates in enzymatic reactions proceed in millisecond and second ranges, the stopped-flow method has been applied to register these processes, which allows mixing an enzyme and substrate for ~1 ms, followed by continuous recording of the fluorescence intensity of various fluorescent markers, whose characteristics are shown below. The registered kinetic curves of changes in fluorescence intensity have reflected conformational transformations during an enzyme–substrate interaction.

$$F = f_0[E] + f_1[ES_1] + f_2[ES_2] + \cdots + f_n[ES_n] + F_{noise} \quad (1)$$

$$\frac{d[ES_1]}{dt} = k_1[S][E] + k_{-2}[ES_2] - (k_{-1} + k_2)[ES_1] \quad (2)$$

$$\frac{d[ES_i]}{dt} = k_i[ES_{i-1}] + k_{-(i+1)}\left[ES_{(i+1)}\right] - (k_{-i} + k_{i+1})[ES_i] \quad (3)$$

$$\frac{d[ES_n]}{dt} = k_n[ES_{n-1}] - (k_{-n} + k_{n+1})[ES_n] \quad (4)$$

$$\frac{d[P]}{dt} = k_{n+1}[ES_n] \quad (5)$$

$$E_0 = [E] + \sum_{i=1}^{n}[ES_i] \quad (6)$$

$$S_0 = [S] + [P] + \sum_{i=1}^{n}[ES_i] \quad (7)$$

An analysis of the kinetic data has been conducted according to Equation (1). The total fluorescence intensity is equal to the sum of the mathematical products of the coefficients of specific fluorescence f and the concentrations of the respective fluorescent species and background fluorescence. Concentrations of all enzyme forms corresponding to the analyzed kinetic scheme have been found via the solution of a system of differential equations and material balance equations (Equations (2)–(7)). A numerical solution of this system of equations using the software enables a researcher to obtain the dependence of concentrations of all reaction intermediates on time, rate constants, and initial concentrations of the interacting substances. During the numerical integration, the values of the rate constants and coefficients of specific fluorescence of all forms are optimized so that the theoretical curve corresponding to this mechanism describes the experimental curve. Using a stepwise increase in complexity of the interaction model, it is possible to discriminate between various schemes of enzyme–substrate interaction and to determine the minimal number of stages in the scheme that will satisfactorily describe the experimental data, judging by the match between the theoretical curve and experimental curve; this match is estimated as a deviation of the difference of these curves (residuals) from a zero line. Figure 2a shows an example of the analysis of a kinetic curve, including the dependence of concentrations of all fluorescently registered reaction intermediates on time. In this case, the stage of accumulation of reaction products was additionally confirmed by direct examination of the accumulation of reaction products by gel electrophoresis. The correspondence of the proposed kinetic scheme to the experimental data is presented in Figure 2b.

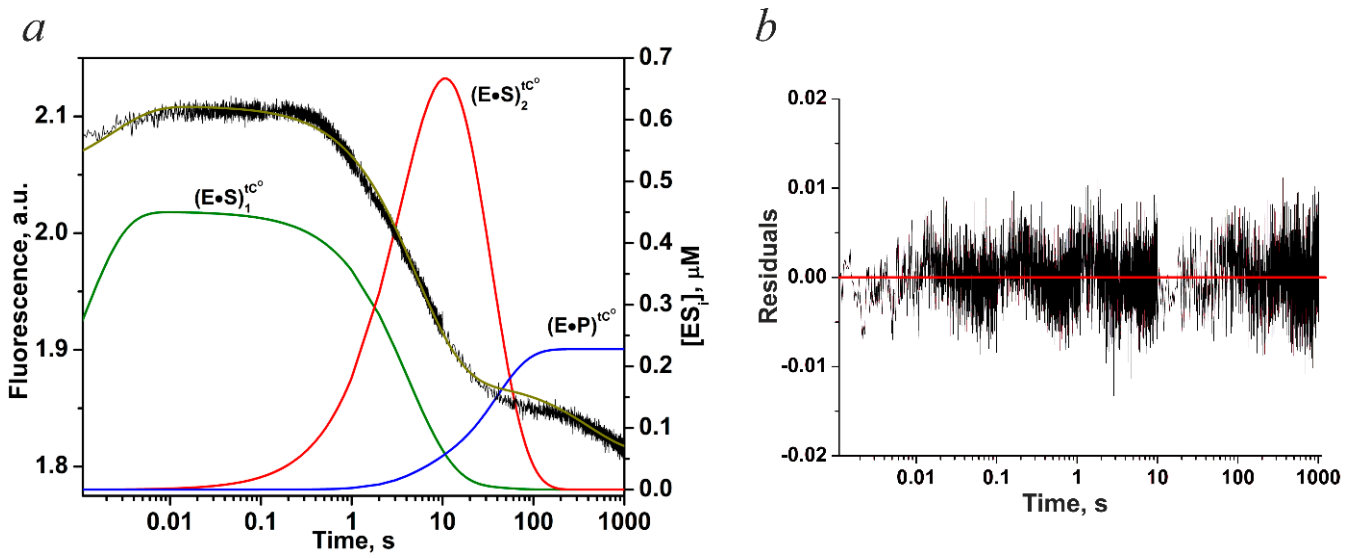

Figure 2. (**a**) The dependence of concentrations of reaction intermediates on time; and (**b**) the deviation of the difference between the theoretical and experimental curves (residuals) from the zero line.

3. Conformational Changes in DNA Glycosylases of the HhH-GPD Structural Family and in DNA during Their Interaction

3.1. Human 8-Oxoguanine DNA Glycosylase hOGG1

Human 8-oxoguanine DNA glycosylase hOGG1 has very high specificity for 8-oxoguanine (oxoG), although it differs from guanine by only two atoms [58–60]. In the case of the oxidized base, the enzyme hydrolyzes the *N*-glycosidic bond and catalyzes the reaction of β-elimination of the phosphate group (Figure 3) [61–65].

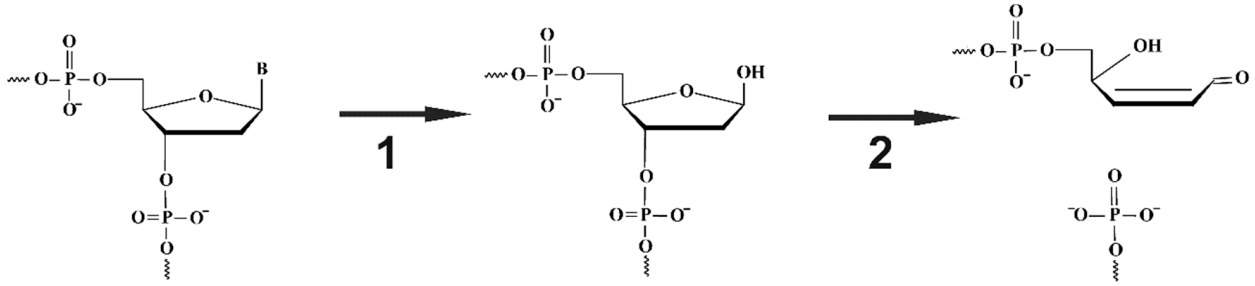

Figure 3. Chemical steps of hOGG1's catalysis (step 1: hydrolysis of the *N*-glycosidic bond and removal of the damaged base resulting in an AP-site; step 2: β-elimination of the 3′-phosphate group).

An analysis of the crystal structures of the enzyme and of its complex with DNA has revealed that both the protein and DNA change their conformation in the catalytic complex. DNA is kinked at the site of the lesion, and the damaged nucleotide is flipped out of the duplex and is located in the active site of the enzyme [66,67]. At the same time, amino acid residues Arg154, Arg204, Asn149, and Tyr203 are intercalated into the cavity that arose in DNA after the base eversion (Figure 4).

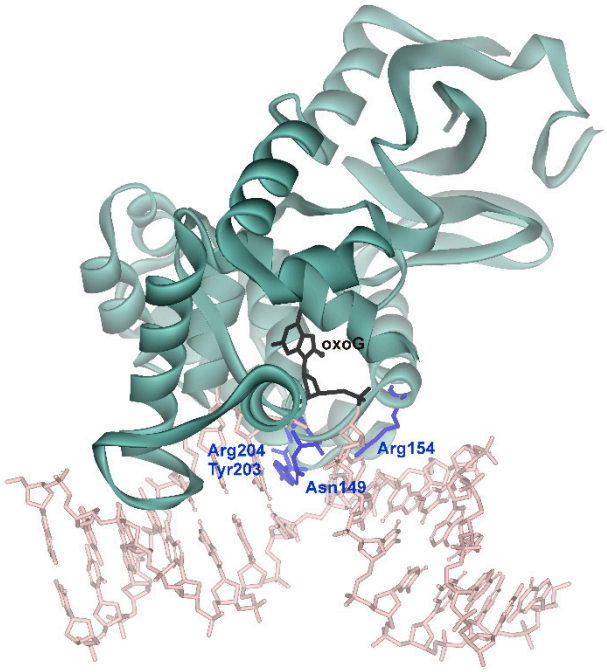

Figure 4. Structure of the complex of enzyme hOGG1 with a DNA duplex containing oxoG (Protein Data Bank [PDB] ID: 1EBM).

To elucidate the function of some amino acid residues of the enzyme in the processes of DNA binding, lesion recognition, and catalytic reaction, mutants of the enzyme have been used [60,64,68–70], which contain substitutions of amino acid residues Tyr203, Arg154, or Arg204 (intercalation into the duplex), Phe45, Phe319, or His270 (boundaries of the pocket in which the everted base is located), and Lys249 or Asp268 (catalytic amino acid residues) (Figure 5). These residues have been replaced by site-directed mutagenesis, and thus mutants of the enzyme have been created. Some of the mutants contain a substitution with a tryptophan residue, which has served as a fluorescent marker in a certain region of the enzyme–substrate complex and helped to register the processes involving the affected amino acid residue.

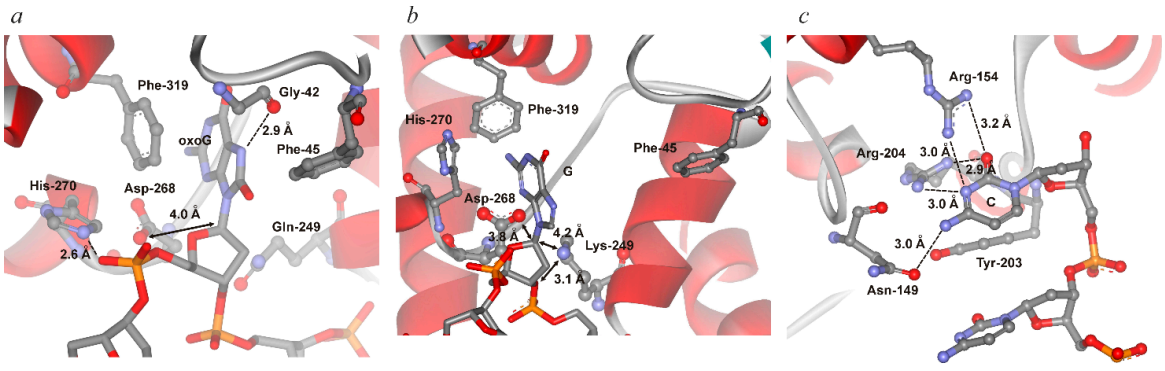

Figure 5. Specific contacts ensuring recognition of a damaged base in the active site of hOGG1. (**a**) The complex of hOGG1 with an oxoG-containing DNA duplex, and the oxoG base is situated in the active site; the image shows the location of amino acid residues Gly42, Phe45, His270, and Phe319 forming the active-site pocket and catalytic residues Asp268 and Gln249 (instead of Lys249) (PDB ID: 1YQR). (**b**) The complex of hOGG1 with an intact DNA duplex, and the G base is located in the exo-site; the image shows the location of amino acid residues Phe45, His270, and Phe319 and catalytic residues Asp268 and Lys249 (PDB ID: 1YQK). (**c**) The complex of hOGG1 with a DNA duplex containing oxoG; the image shows amino acid residues Asn149, Arg154, Tyr203, and Arg204 (PDB ID: 1EBM).

Relative catalytic activity of the mutant enzymes during the interaction with an oxoG-substrate has been determined by direct examination of the reaction products' accumulation by gel electrophoresis (Figure 6) [68–70]. Substitution of catalytic amino acid residues Lys249 and Asp268 leads to a complete loss of *N*-glycosylase and AP-lyase activities. Furthermore, substitutions of amino acid residues getting intercalated into the DNA duplex (Tyr203Ala, Arg154Ala, and Arg204Ala) and of His270Trp cause a significant decrease in catalytic activity.

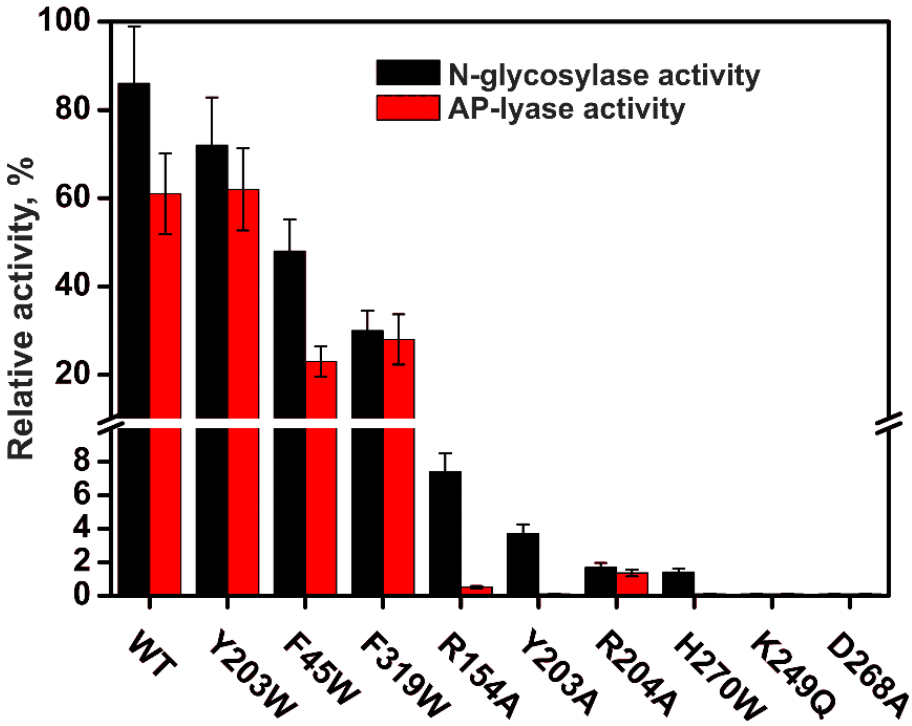

Figure 6. Relative activity of wild-type hOGG1 and mutants of this enzyme. Analysis of products of the *N*-glycosylase reaction and of β-elimination after 15 min of the interaction of wild-type hOGG1 or one of its mutants with oxoG-substrate.

Changes in fluorescence intensity of Trp residues during the binding of wild-type or mutant hOGG1 to an intact DNA duplex, even after the introduction of new tryptophan residues, have been too weak for their correct quantitative analysis (Figure 7a) [68]. This finding indicates that the enzyme molecule does not undergo appreciable conformational rearrangements during the formation of the initial nonspecific complex with undamaged DNA. By contrast, a significant increase in fluorescence intensity of aPu, as registered with an undamaged DNA duplex containing aPu residue, unequivocally points to disruption of Watson–Crick bonds and/or of stacking during the emergence of the nonspecific enzyme–DNA complex (Figure 7b) [68].

In addition, according to [60,71,72], at this point, the G base may undergo partial eversion from the double helix and insertion into the exo-site of the enzyme. Differences in the amplitude and timing of the signal change reflect a difference between the mutant versions of the enzyme in the ability to bind intact DNA and different degrees of duplex loosening by these mutants. Typically, substitutions lead to the deceleration of the complex formation and decrease its stability.

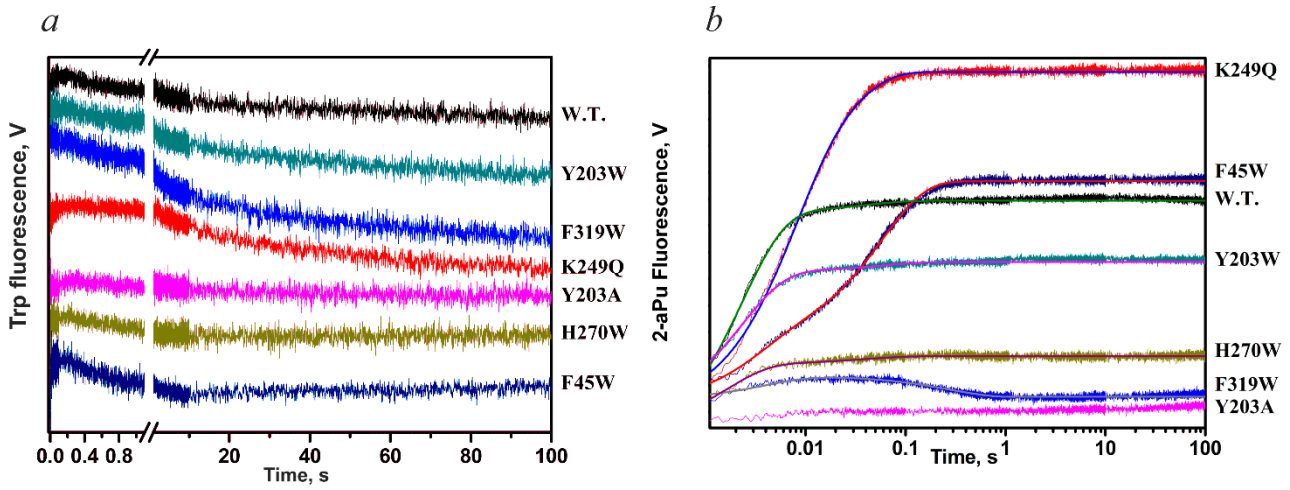

Figure 7. Conformational alterations in the enzyme and DNA during the formation of the initial nonspecific complex. Changes in fluorescence intensity of Trp (**a**) and aPu (**b**) during interaction of wild-type hOGG1 or one of its mutants with intact DNA duplex or with undamaged DNA duplex containing aPu residue. Concentrations of hOGG1 and DNA ligands were 2.0 and 1.0 μM, respectively.

In the course of interaction with a substrate containing an AP site, the fluorescence intensity of Trp in mutants of hOGG1 slowly decreases during 10 s (Figure 8a) [64,68]. Because hOGG1 catalyzes the β-elimination reaction (AP-lyase activity) with very low efficiency, this decrease in Trp fluorescence likely reflects only the DNA-binding step. The binding of an AP-substrate containing an aPu residue and the intercalation of amino acid residues of hOGG1 into the DNA duplex give well-pronounced aPu fluorescence changes characterizing DNA conformational transitions (Figure 8b) [60,68]. A slight increase in fluorescence intensity of aPu (before time point 100 ms) for wild-type hOGG1 and all mutants is likely related to enhancement of the hydrophilicity of the medium near the aPu residue. This increase is most likely due to partial melting of the duplex and/or interactions with hydrophilic residues Arg154, Arg204, and Asn149. Additionally, these data suggest that substitution of Tyr203Trp leads to a slowdown of the decline phase, whereas substitution of Tyr203Ala eliminates this phase altogether. That is, the process that induces the diminution of fluorescence intensity is related to the intercalation of Tyr203 into DNA.

Equation (8) has been utilized to calculate the observed rate constants characterizing the change in fluorescence intensity during the interaction with intact DNA duplex and with AP-substrate:

$$F_c = F_b + \sum_{i=0}^{N} A_i \times \exp(-k_i \times t) \quad (8)$$

where i is a stage number, A_i is the amplitude of the signal change, and k_i is the observed rate constant.

Interaction between wild-type hOGG1 and a DNA duplex containing oxoG results in a decline of the signal of Trp fluorescence within 10 s (Figure 9a) [68]. Earlier, it was demonstrated [64] that this phase includes three equilibrium stages related to the formation of the enzyme–DNA catalytic complex (Scheme 1). The subsequent rise in intensity of Trp fluorescence can be explained by the chemical steps of the enzymatic process and by the dissociation of the enzyme–product complex. The interaction between wild-type hOGG1 and an oxoG-substrate containing aPu residue yields an increase in aPu fluorescence intensity during the first 20 ms (Figure 9b) [68]. According to [60], within this time interval, the oxoG base is flipped out of the duplex into the active site of the enzyme, thereby leaving free space in the duplex. At the next step, between time points 20 ms and 100 s, a two-phase decrease in the fluorescence of aPu occurs, characterized by the sequential intercalation of

residues Tyr203, Asn149, Arg154, and Arg204 into this DNA-free space. Catalytic steps and dissociation of the enzyme–product complex cause an increase in the fluorescence intensity of aPu at time points after 100 s.

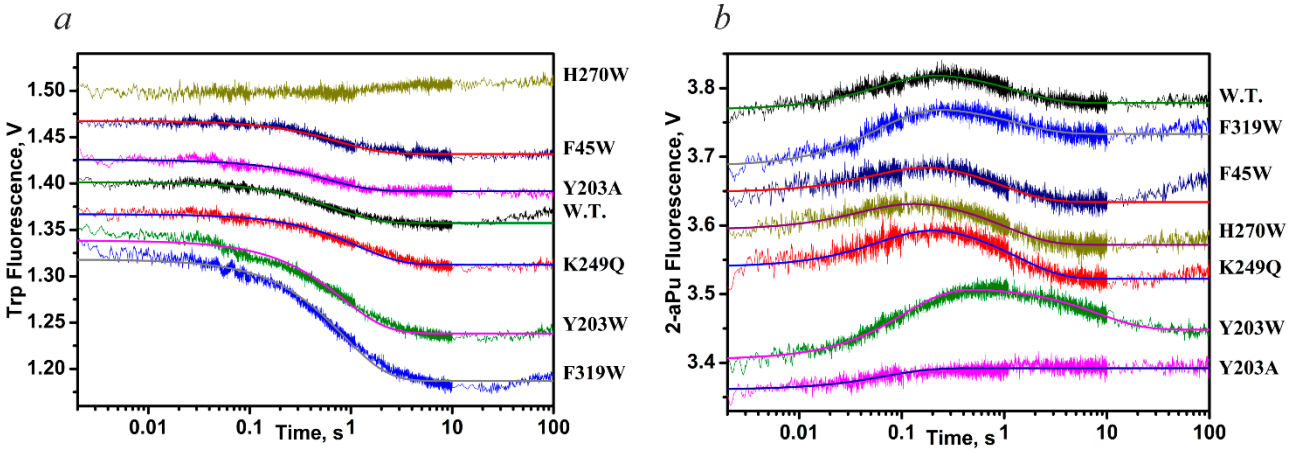

Figure 8. Experimental and theoretical kinetic curves reflecting conformational changes in the enzyme (**a**) and DNA substrate (**b**) during the interaction of wild-type hOGG1 or one of its mutants with DNA duplexes, which contain an AP-site. Concentrations of hOGG1 and of the DNA substrates were 2.0 and 1.0 μM, respectively.

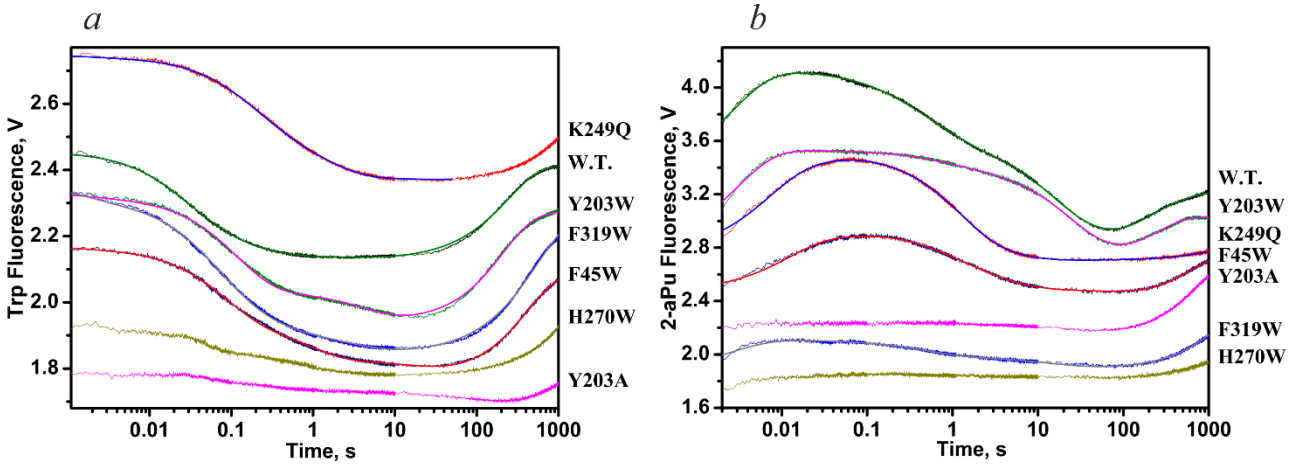

Figure 9. Experimental and theoretical kinetic curves characterizing conformational alterations of the enzyme (**a**) and of a DNA substrate (**b**) during the interaction of wild-type hOGG1 or one of its mutants with DNA duplexes that contain oxoG. The concentrations of hOGG1 and DNA substrates were 2.0 and 1.0 μM, respectively.

$$E + OG \underset{k_{-1}}{\overset{k_1}{\rightleftarrows}} (E{\bullet}OG)_1 \underset{k_{-2}}{\overset{k_2}{\rightleftarrows}} (E{\bullet}OG)_2 \underset{k_{-3}}{\overset{k_3}{\rightleftarrows}} (E{\bullet}OG)_3 \xrightarrow{k_4} (E{\bullet}AP) \xrightarrow{k_5} (E{\bullet}P \overset{K_p}{\rightleftarrows} E + P)$$

Scheme 1. Kinetic mechanism of interaction between hOGG1 and oxoG-containing DNA substrate.

E is hOGG1; OG is oxoG-substrate; $(E{\bullet}OG)_n$ are various enzyme–substrate complexes arising during the recognition of 8-oxoguanine; E•AP is a complex of E with an AP-site resulting from an *N*-glycosylase reaction; E•P is a complex of E with reaction product P generated by an AP-lyase reaction; k_i and k_{-i} are rate constants of the forward and reverse reactions of the individual steps.

Taken together, these findings show that the selected amino acid residues indeed take part in both the nonspecific binding and subsequent damage recognition because they all affect conformational alterations in both the enzyme and the duplex. For all mutants of the enzyme, concentration series of kinetic curves have been obtained characterizing changes in the fluorescence of Trp and aPu, and kinetic parameters of the individual stages have been calculated (Table 1).

Thermodynamic analysis of the interaction of hOGG1 with damaged and undamaged DNA has been performed on the basis of kinetic data generated at different temperatures. As the temperature decreases, the catalytic activity of the enzyme decreases considerably (Figure 10a) [72]. The kinetic curves (Figure 10b) describing the formation of a nonspecific complex at low temperatures contain two distinct phases of fluorescence intensity growth, implying a two-stage interaction mechanism. For each temperature, a concentration series has been obtained, allowing the calculation of individual rate constants of forward and reverse reactions in equilibrium stages (Table 2).

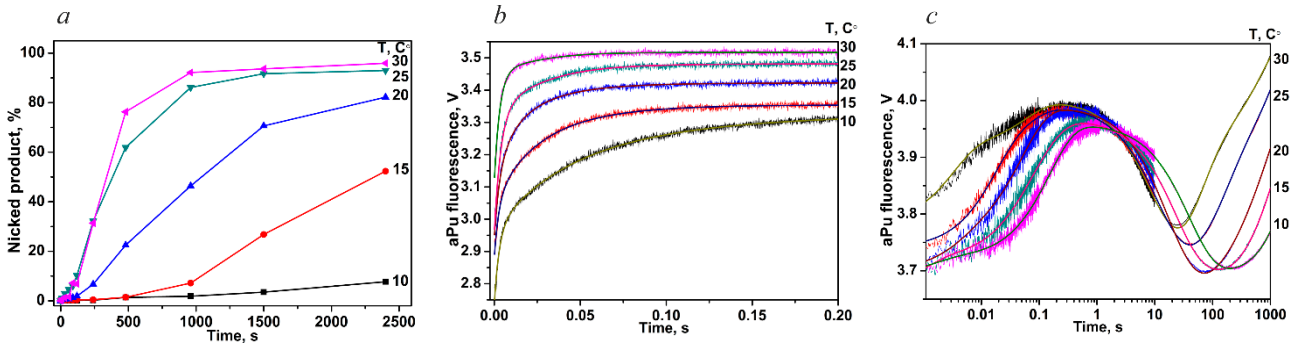

Figure 10. Catalytic efficiency of hOGG1 toward oxoG-substrate at different temperatures monitored by PAGE (**a**). Changes in fluorescence intensity of aPu during the interaction of hOGG1 with undamaged DNA (**b**) or oxoG-substrate (**c**) at different temperatures.

Table 1. Rate and equilibrium constants characterizing the interaction of wild-type hOGG1 or its mutants with a DNA substrate containing oxoG, as determined by the analysis of changes in fluorescence intensity of Trp and aPu.

	Trp Detection					**aPu Detection**				
Constants	**WT**	**K249Q**	**Y203W**	**F319W**	**F45W**	**WT**	**K249Q**	**Y203W**	**F319W**	**F45W**
$k_1 \times 10^{-8}$, $M^{-1}s^{-1}$	2.6 ± 0.1	1.7 ± 0.4	5.4 ± 1.0	2.2 ± 0.1	6.9 ± 1.8	1.2 ± 0.1	0.3 ± 0.1	0.66 ± 0.04	0.6 ± 0.2	0.5 ± 0.1
k_{-1}, s^{-1}	130 ± 1	290 ± 60	520 ± 110	240 ± 10	500 ± 45	120 ± 10	62 ± 12	130 ± 7	260 ± 40	103 ± 9
K_1, M^{-1}	2.0×10^6	0.6×10^6	1.0×10^6	0.9×10^6	1.4×10^6	1.0×10^6	0.5×10^6	0.5×10^6	0.2×10^6	0.5×10^6
k_2, s^{-1}	13.3 ± 0.2	5.0 ± 0.5	7.4 ± 1.0	31.9 ± 1.2	12.1 ± 2.0	1.4 ± 0.1	1.4 ± 0.1	0.3 ± 0.1	4.1 ± 1.5	1.4 ± 0.1
k_{-2}, s^{-1}	1.16 ± 0.02	2.8 ± 0.2	1.2 ± 0.2	0.5 ± 0.1	2.3 ± 0.6	1.5 ± 0.1	1.1 ± 0.2	1.3 ± 0.3	2.5 ± 0.8	1.4 ± 0.2
K_2	11.5	1.8	6.2	63.8	5.3	0.9	1.3	0.2	1.6	1.0
k_3, s^{-1}	0.012 ± 0.001	0.26 ± 0.01	0.010 ± 0.001	0.08 ± 0.01	0.009 ± 0.001	0.10 ± 0.01	5.4 ± 1.1	0.28 ± 0.04	0.9 ± 0.2	0.48 ± 0.09
k_{-3}, s^{-1}	0.07 ± 0.01	0.52 ± 0.01	0.12 ± 0.01	0.8 ± 0.1	0.4 ± 0.1	0.013 ± 0.002	0.8 ± 0.1	0.022 ± 0.008	0.5 ± 0.2	0.38 ± 0.04
K_3	0.17	0.5	0.08	0.1	0.02	7.7	6.7	12.7	1.8	1.3
k_4, s^{-1}	0.06 ± 0.02	-	0.03 ± 0.01	0.018 ± 0.002	0.05 ± 0.01	0.029 ± 0.001	-	0.015 ± 0.004	0.015 ± 0.004	0.034 ± 0.002
$k_5 \times 10^3$, s^{-1}	6.4 ± 0.7	-	4.2 ± 0.9	1.8 ± 0.1	0.4 ± 0.1	3.6 ± 0.2	-	3.0 ± 0.7	1.9 ± 0.1	4.4 ± 0.1
K_{EP}, μM	0.88	-	0.3 ± 0.1	1.1 ± 0.1	1.3 ± 0.4	7.0 ± 1.1	-	1.0 ± 0.2	-	-
K_{bind}, M^{-1}	2.9×10^7	2.2×10^6	8.0×10^6	6.5×10^7	8.8×10^6	9.2×10^6	5.3×10^6	2.1×10^6	1.3×10^6	1.6×10^6
$K_1 \times K_2 \times K_3$	3.9×10^6	0.54×10^6	0.50×10^6	6.1×10^6	0.15×10^6	6.9×10^6	4.3×10^6	1.3×10^6	0.58×10^6	0.65×10^6

$K_i = k_i / k_{-i}$, $K_{bind} = K_1 + K_1 \times K_2 + K_1 \times K_2 \times K_3$

Table 2. Rate constants describing the interaction of wild-type hOGG1 with undamaged DNA or oxoG-substrate at different temperatures.

DNA	Constants	Temperature				
		10 °C	**15 °C**	**20 °C**	**25 °C**	**30 °C**
oxoG-substrate	k_1, $M^{-1}s^{-1}$	$(1.3 \pm 0.7) \times 10^7$	$(2.2 \pm 1.0) \times 10^7$	$(1.7 \pm 0.8) \times 10^7$	$(1.9 \pm 1.0) \times 10^7$	$(2.0 \pm 1.0) \times 10^7$
	k_{-1}, s^{-1}	230 ± 80	390 ± 50	360 ± 20	410 ± 70	520 ± 120
	k_2, s^{-1}	8.3 ± 3.8	15.6 ± 4.2	26.6 ± 6.0	53.5 ± 20.3	72.4 ± 31.4
	k_{-2}, s^{-1}	6.1 ± 0.2	11.8 ± 0.2	19.6 ± 1.7	37.9 ± 11.1	40.5 ± 12.5
	k_3, s^{-1}	0.087 ± 0.017	0.12 ± 0.03	0.19 ± 0.07	0.4 ± 0.1	0.3 ± 0.1
	k_{-3}, s^{-1}	0.011 ± 0.001	0.018 ± 0.001	0.007 ± 0.002	0.02 ± 0.003	0.002 ± 0.001
	k_4, s^{-1}	0.005 ± 0.001	0.007 ± 0.001	0.014 ± 0.002	0.026 ± 0.003	0.041 ± 0.007
	k_5, s^{-1}	0.0006 ± 0.0001	0.0012 ± 0.0001	0.001 ± 0.0001	0.001 ± 0.001	0.0037 ± 0.007
undamaged DNA	k_1, $M^{-1}s^{-1}$	$(5.6 \pm 1.2) \times 10^7$	$(6.6 \pm 1.1) \times 10^7$	$(5.9 \pm 1.3) \times 10^7$	$(6.3 \pm 0.3) \times 10^7$	$(7.4 \pm 1.4) \times 10^7$
	k_{-1}, s^{-1}	97 ± 23	128 ± 21	119 ± 19	140 ± 14	170 ± 17
	k_2, s^{-1}	12.6 ± 5.5	17.5 ± 2.2	20.7 ± 6.3	14.0 ± 1.5	18.2 ± 8.7
	k_{-2}, s^{-1}	12.4 ± 0.5	25.2 ± 1.3	38.9 ± 1.9	49.8 ± 2.3	72.1 ± 9.9

Kinetic curves reflecting the interaction of hOGG1 with substrate with oxoG-substrate have a more complicated profile: rise-fall-rise (Figure 10c) [72]. The concentration series of kinetic curves obtained by recording the fluorescence intensity of aPu for each temperature is described in Scheme 1, enabling us to calculate the rate constants (Table 2).

By means of the values of the rate constants of forward and reverse reactions, for each *i*-th equilibrium stage, equilibrium constants (K_i) have been computed. The dependence of $ln(K_i)$ on 1/T has a linear shape (Figure 11a), and with the help of the Van't Hoff equation (Equation (9)), we can calculate the standard enthalpy ΔH_i° and entropy ΔS_i° of all equilibrium stages (Table 3). From the temperature dependence of the irreversible stages' rate constants that characterize the hydrolysis of the *N*-glycosidic bond (k_4) and the β-elimination reaction (k_5) (Figure 11b), standard activation enthalpy ($\Delta H^{\circ,\ddagger}$) and standard activation entropy ($\Delta S^{\circ,\ddagger}$) are calculated. This dependence is described by the Eyring equation (Equation (10)) for the transition state theory.

$$\ln(K_i) = -\Delta G_i^\circ/RT = -\Delta H_i^\circ/RT + \Delta S_i^\circ/R, \quad (9)$$

where ΔG_i° is standard Gibbs free energy, ΔH_i° is standard enthalpy, and ΔS_i° is standard entropy.

$$\ln(k_i/T) = \ln(k_B/h) + \Delta S^{\circ,\ddagger}/R - \Delta H^{\circ,\ddagger}/RT, \quad (10)$$

where k_B and h are respectively Boltzmann and Planck constants, R is the gas constant, T is the absolute temperature in Kelvin degrees, and k_i is the rate constant of the chemical step.

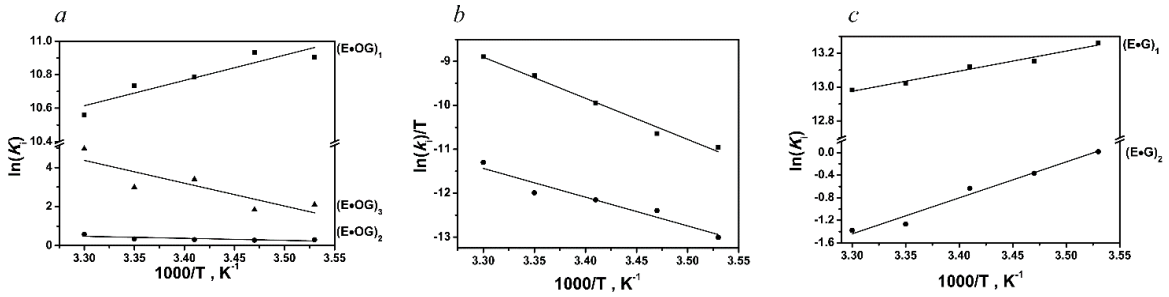

Figure 11. The dependence of $\ln(K_i)$ (**a**,**c**) and of $\ln(k_i/T)$ (**b**) on 1/T according to the Van't Hoff and Eyring equations, which characterize the interaction of wild-type hOGG1 with substrate oxoG-substrate (**a**,**b**) or undamaged DNA (**c**).

Table 3. Thermodynamic parameters of the interaction of wild-type hOGG1 with undamaged DNA or oxoG-substrate.

DNA	Parameter / Stage Number	ΔG°_{i298}, kcal/mol	ΔH°_{i}, kcal/mol	ΔS°_{i}, cal/(K·mol)
oxoG-substrate	1	−6.4	−2.8 ± 0.7	11.2 ± 2.4
	2	−0.2	2.1 ± 0.9	7.7 ± 3.3
	3	−1.8	23.2 ± 7.8	85.4 ± 26.6
	$\sum_{i=1}^{i=3}$	−8.4	22.5 ± 9.4	104.3 ± 32.3
	4	19.6	18.6 ± 1.1	−3.5 ± 3.9
	5	21.0	13.0 ± 1.9	−27.0 ± 6.7
undamaged DNA	1	−7.7	−2.4 ± 0.2	18.0 ± 0.7
	2	0.8	−12.7 ± 1.2	−44.7 ± 4.1
	$\sum_{i=1}^{i=2}$	−6.9	−15.1 ± 1.4	−26.7 ± 4.8

The mechanism of incision of damaged DNA includes the sequential formation of covalent intermediate complexes of the enzyme with DNA in the form of a Schiff base (Figure 12). To determine characteristic times of the emergence and disappearance of these intermediates, electrospray ionization mass spectrometric analysis of the reaction mixture is performed at certain time intervals (Figure 13) [53], while $NaBH_4$ is added to the reaction mixture to reduce the Schiff base at 0–1000 s after the start of the reaction.

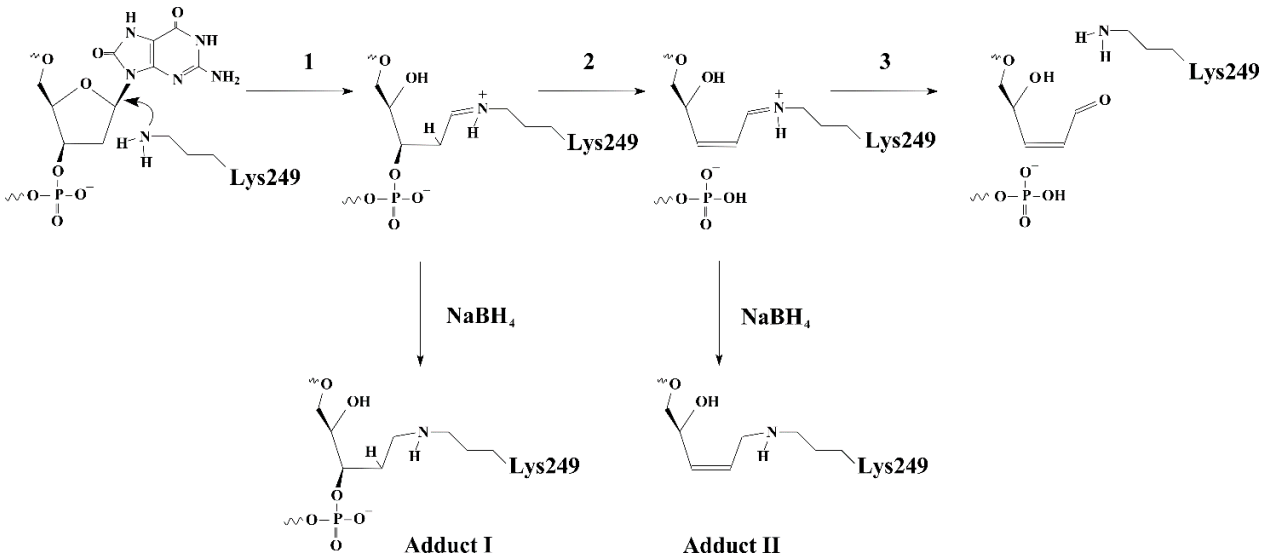

Figure 12. The main reaction steps catalyzed by hOGG1. Step 1: removal of the damaged base (*N*-glycosidic bond hydrolysis); step 2: the reaction of β-elimination of the 3′-phosphate group; step 3: regeneration of the free enzyme. Stable covalent adducts are depicted that come into being after reduction of the Schiff base by $NaBH_4$.

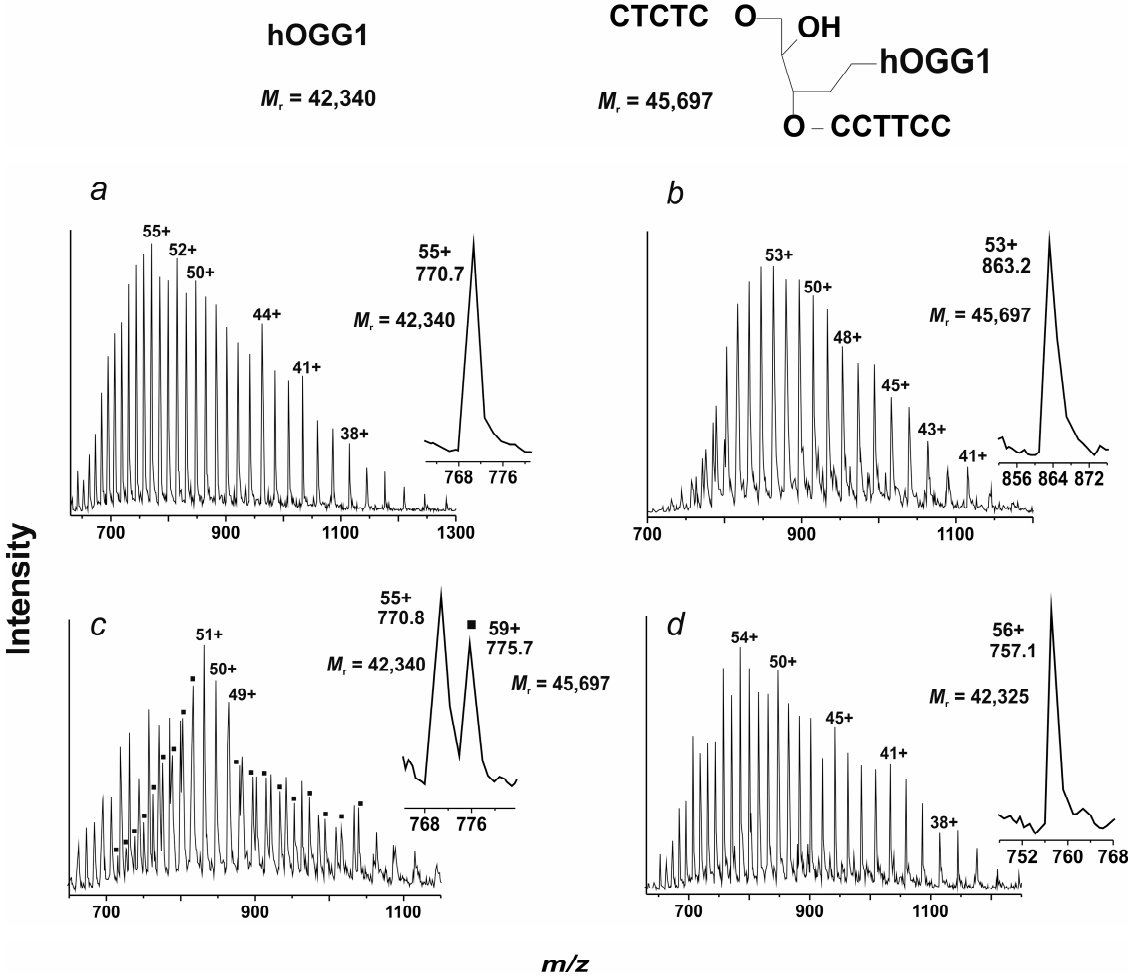

Figure 13. MS/ESI spectra of intermediates arising during the interaction of enzyme hOGG1 and oxoG-substrate at t = 0, 30, 600, and 1000 s ((**a**–**d**), respectively).

The mass spectrum of the free enzyme hOGG1 contains a set of positively charged ion peaks that match the molecular weight of the unmodified protein (42,340 Da) (Figure 13a). During the first 30 s, the *N*-glycosylase reaction proceeds and adduct I is produced (Figure 13b). Adduct II, corresponding to the covalent complex with DNA after the β-elimination of the 3′-phosphate group, has been undetectable. The mass spectra show slow regeneration of the free enzyme from the complex corresponding to adduct I. This evidence confirms that the rate-limiting step is the β-elimination reaction.

A combined analysis of the mass spectrometric data, thermodynamic parameters, and mutational analysis results obtained from the interaction with damaged and undamaged DNA allows us to conclude that the first stage of the interaction is the formation of a nonspecific complex, accompanied by the "melting" of DNA duplex strands, as follows from the increasing intensity of aPu fluorescence. Moreover, X-ray diffraction analysis indicates partial eversion of an intact base from the helix in such a nonspecific complex.

This stage has values of thermodynamic parameters that are similar for damaged and undamaged DNA and is characterized by energetically favorable changes in enthalpy and entropy (Table 3). At this stage, DNA is scanned for damage by hOGG1 via the insertion of a so-called wedge into the DNA double helix, which is Tyr203. Furthermore, it is reported that each substitution of Arg154Ala and Arg204Ala significantly lowers the activity of the enzyme owing to the loss of the ability to locally disrupt the structure of the duplex, suggesting that these residues directly participate in this stage of the interaction. Kinetic evidence indicates that catalytic amino acid residue Lys249 also participates in the duplex

loosening and eversion of oxoG by means of electrostatic interactions with phosphate groups of the nucleotide, and contacts with His270 are also important at this stage.

The second stage of damage recognition is energetically neutral, and the loss of enthalpy is compensated by an increase in entropy. At this stage, a bond forms between His270 and the phosphate group of the damaged nucleotide, thereby facilitating a shift of oxoG to the active site of the enzyme, where it engages in a stacking interaction with Phe319. In addition, intercalation of Arg154, Arg204, and Asn149 into the DNA helix takes place at this stage. In the case of an intact duplex, this step is absent; therefore, this step is important for discrimination between damaged and undamaged bases.

The last, third stage of recognition gives rise to a catalytically competent conformation of hOGG1. At this stage, the oxoG base is completely within the active site, where the local rearrangements happen that are necessary to implement the hydrolysis of the *N*-glycosidic bond. In this context, the formation of the catalytic complex features high endothermicity due to the enthalpy change, which is compensated by a substantial increase in entropy. The growth of entropy during an interaction of DNA-binding proteins with DNA is usually due to two factors: desolvation of polar groups in the region of the protein–DNA contact and displacement of highly ordered "crystalline" water molecules from DNA grooves. Accordingly, the formation of a catalytically competent state requires dehydration of the protein–DNA interface and the assembly of a more compact enzyme–substrate complex. After that, catalytic stages of the enzymatic process occur, and the dissociation of the enzyme–product complex completes the enzymatic cycle.

3.2. Other Members of the HhH-GPD Structural Family: MutY, MBD4, and Nth

Enzymes in the HhH-GPD structural family have considerable differences both in size and in the general layout of the protein globule [73]. Such dissimilarities are attributable, among other things, to the specific functions of these enzymes. For example, the *adenine-DNA glycosylase MutY* from *Escherichia coli* possesses unique specificity for the oxoG/A pair, forms an elaborate network of contacts with both DNA strands, and at the same time hydrolyzes the *N*-glycosidic linkage to the intact adenine base located opposite the oxoG [74–76]. Moreover, the removal of adenine from the G/A pair is ~10 times less efficient, which confirms the high efficiency of discrimination at a specific site in DNA. Kinetics of the interaction with model DNA substrates and with ligands have been recorded by means of changes in fluorescence intensity of Trp residues and of a fluorescein residue in DNA [77,78]. It has been found that during the formation of the initial complex, nonspecific contacts emerge between the DNA-binding site of the enzyme and the DNA duplex. At the second stage of the interaction of MutY with the DNA substrate, discrimination of bases G and oxoG located opposite adenine takes place, as does recognition of adenine itself and the formation of a catalytic complex.

Another representative of the HhH-GPD structural family, *human methyl-CpG-binding domain 4 (MBD4)*, contains an *N*-glycosylase catalytic domain that interacts mostly with the damaged DNA strand and removes uracil [79,80]. To analyze conformational transformations during the enzymatic process, model substrates containing various fluorophores, including new ones, have been screened [81]. It has been shown that fluorophores are not always sensitive enough to the duplex structure alterations induced by the enzyme. As the most sensitive fluorescent markers of the enzymatic process, we have chosen Trp and aPu residues and the FRET pair FAM/BHQ1. When fluorescently labeled substrates have been tested, it has been found that the bending of the DNA duplex and its local melting occur in the initial complex. At the next time point, the damaged nucleotide is everted out of the duplex, and amino acid residues Arg468 and Leu508 get inserted into the formed cavity. A catalytic complex forms, in which the hydrolysis of the linkage to uracil takes place, as does the subsequent dissociation of the enzyme's complex with the product.

Another member of this family, *endonuclease III Nth* from *Escherichia coli*, is responsible for the removal of oxidized and reduced pyrimidine bases, such as 5,6-dihydrouracil (DHU) [82]. Although Nth contains two Trp residues, it has not been possible to register

conformational changes in the enzyme during its interaction with DNA [44,83]. Fluorophores and their various locations have been screened for the purpose of registering DNA conformational transformations [44,83]. The most fluorescently sensitive model systems containing DHU, AP site, or F-site as damaged nucleotides and 3′-placed aPu, **X-aPu/G,** and **X/tC^{O}** (X = DHU, AP site, F-site, or G) have been chosen and exploited, which contain various modified nucleotides to which Nth has different specificity. A cumulative analysis of the obtained data [44,83] has revealed that DNA undergoes multiple conformational transformations during the formation of the enzyme–substrate complex. A decline in fluorescence intensity of the new fluorophore tC^{O} and a rise for aPu in the initial part of the kinetic curves signify destabilization of the double helix, which can occur due to local melting, bending of the duplex, or the insertion of residue Leu81 and an attempt to flip the damaged nucleotide out of the duplex. Next, the transition of aPu into a hydrophobic environment, accompanied by a decrease in fluorescence intensity, indicates the intercalation of an active-site amino acid residue into the double helix, which occurs after complete eversion of the damaged nucleotide. According to X-ray diffraction data, this residue is Gln41 [84,85]. After that, an adjustment of the active site takes place, as do the formation of a catalytically competent state, catalytic stages, and dissociation of the enzyme–product complex.

3.3. The General Model of Lesion Recognition by Enzymes of Structural Family HhH-GPD

For all enzymes of this family, with the tested types of DNA substrates and DNA ligands, concentration series have been obtained, kinetic schemes of interaction have been established, and rate constants of these schemes have been calculated [86]. This analysis of the kinetic data shows that, just as in hOGG1, in the enzymes MutY, MBD4, and Nth, the formation of the catalytically competent complex proceeds through a sequence of stages accompanied by conformational alterations of the protein and DNA molecules. The interaction can be broken down into two key steps: (i) the initial nonspecific binding, which also occurs upon interaction with intact DNA; and (ii) the emergence of specific contacts and damage recognition (Table 4).

Table 4. Key steps in the recognition of damage by enzymes of structural family HhH-GPD.

		hOGG1	**Nth (*B. st.*)**	**MBD4**	**MutY (*E. coli*)**
Initial binding	Destabilization of double helix	Arg154, Arg204	Arg78, Arg84	Arg468	Arg50, Arg91
	Intercalation of “sensor”	Tyr203	Leu82	Leu508	Tyr88
Specific recognition	Complete eversion of damaged base	+	+	+	+
	Intercalation of other amino acid residues	Asn149	Gln42	-	Gln48

At the step of nonspecific binding, hydrogen bonds form between a nucleotide (located in the complementary strand opposite the base to be removed) and arginine residues (Arg154 and Arg204 in hOGG1, Arg78 and Arg84 in Nth, and possibly Arg468 in MBD4); this event induces destabilization of the Watson–Crick hydrogen bonds in the damaged segment of the DNA duplex. It should be noted that arginine residues in different enzymes are positioned differently; for instance, when comparing the structures of hOGG1 and Nth, one can see (Figure 14a) that these are structurally nonhomologous residues; nevertheless,

these residues can perform the very same function of destabilizing the damaged segment of the double helix.

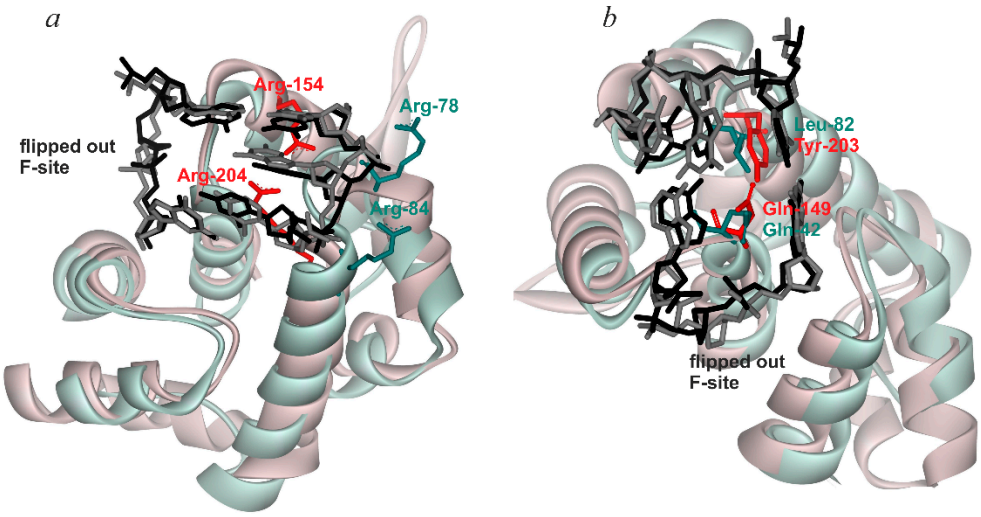

Figure 14. A comparison of spatial structure between DNA-binding sites of hOGG1 (pink, PDB ID 1FN7) and Nth from *Geobacillus stearothermophilus* (greenish, PDB ID 1P59) complexed with F-site-containing DNA. (**a**) Arginine residues interacting with phosphate groups of the complementary DNA strand. Arg154 and Arg204 of hOGG1 are highlighted in red, whereas Arg78 and Arg84 of Nth are highlighted in green. (**b**) Spatial correspondence of residues Tyr203 and Gln149 (red) in hOGG1 to residues Leu82 and Gln42 (green) in Nth.

Furthermore, at this stage, the sensor residue (Tyr203 in hOGG1, Leu81 in Nth, Tyr88 in MutY, and possibly Leu508 in MBD4) is wedged into the DNA duplex destabilized by the arginine residues. If we compare hOGG1 and Nth as an example, one can see (Figure 14b) that these are homologous residues. This intercalation of the amino acid residue induces partial eversion of the damaged base from the DNA strand. This partial eversion into the so-called exo site of the enzyme has been documented crystallographically for hOGG1 (PDB ID 1YQK). In hOGG1, the partially inverted base is reported to come into contact with His270 and Lys249 (Lys120 in Nth).

At the stage of specific binding in the case of hOGG1, oxoG is completely everted into the active-site pocket of the enzyme with the initiation of stacking with the aromatic ring of Phe319, followed by the final formation of contacts between the Cyt base and residues Arg154, Arg204, and Asn149, which are intercalated into the duplex. In Nth, these residues are Arg78, Arg84, and Gln41, whereas in MutY, they are Gln48 and possibly Arg50 and Arg91. Known structures of the MBD4 catalytic domain cannot help identify the amino acid residue that performs the function of Asn or Gln in other members of the HhH-GPD family. The complete intercalation of these residues into the DNA double helix is accompanied by final conformational fine-tuning of the enzyme–substrate complex, resulting in a catalytically competent state.

4. Conformational Alterations in DNA Glycosylases of Structural Family H2tH and in DNA during Their Interaction

4.1. Endonuclease VIII Nei

Endonuclease VIII Nei is one of the main DNA glycosylases in prokaryotic cells and removes a wide range of oxidized or reduced pyrimidine bases [87,88] (Figure 15). Analysis of X-ray diffraction data [89,90] indicates that in the enzyme–substrate complex, the N- and C-terminal domains of the enzyme undergo closure, the sugar-phosphate backbone of DNA gets kinked, the damaged base is flipped out of the duplex and is located in the active site of the enzyme, and the triad of residues Gln69, Leu70, and Tyr71 gets inserted into the nascent cavity (Figure 16a).

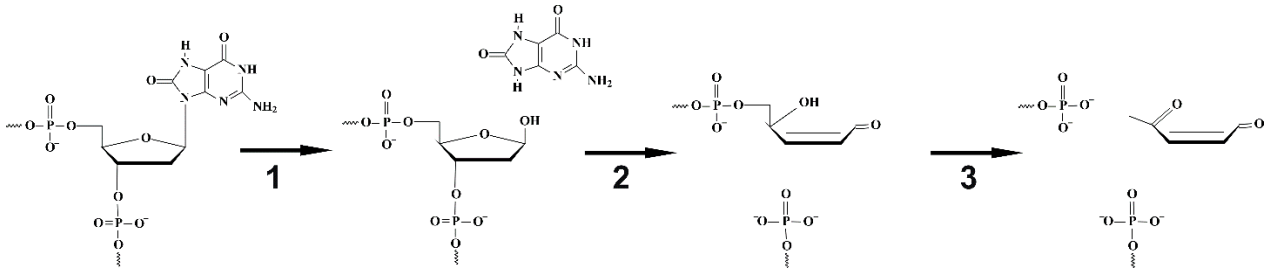

Figure 15. Chemical steps of Nei's catalysis. Step 1: hydrolysis of the *N*-glycosidic bond and removal of the damaged base, resulting in an AP-site; stage 2: β-elimination of the 3′-phosphate group; step 3: β-elimination of the 5′-phosphate group.

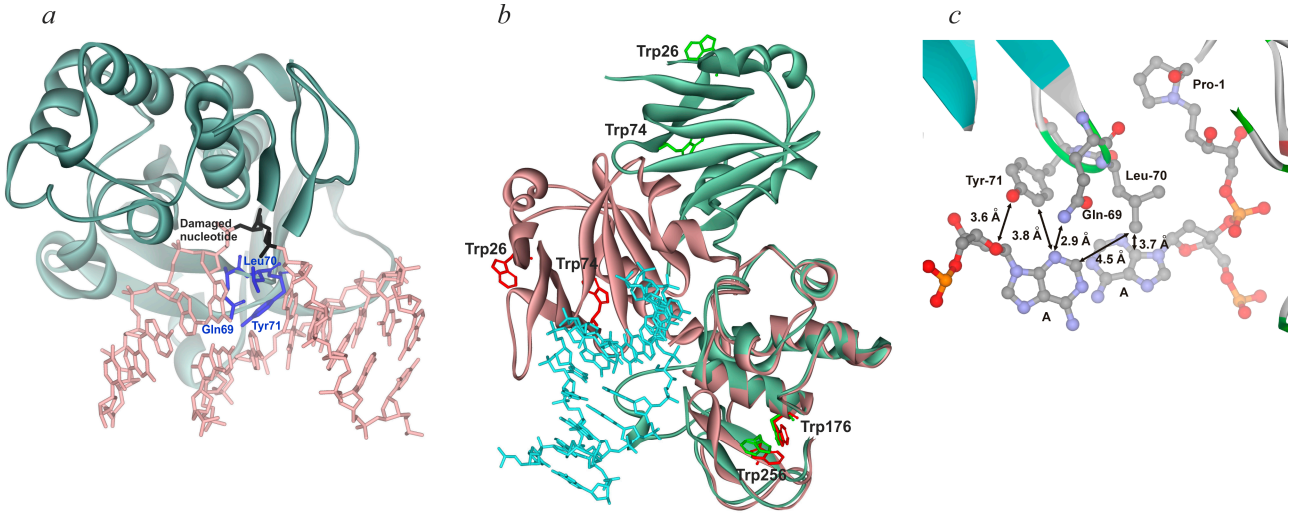

Figure 16. Schematic representation of spatial structure of the complex of enzyme Nei with DNA. (**a**) Structure of the covalent complex of Nei with a DNA duplex containing an AP-site (PDB ID 1K3W). (**b**) Spatial distribution of Trp residues and conformational changes associated with formation of enzyme-DNA complex. (**c**) Functionally important amino acid residues taking part in the formation of specific contacts between the enzyme and DNA.

Enzyme Nei contains four Trp residues (Figure 16b), which have been employed [91] to register conformational changes in the enzyme during DNA binding. Scheme 2 has been proposed, according to which the initial DNA binding happens at the first stage, whereas the DNA bending, the eversion of the lesion, the insertion of the triad of amino acid residues, and the assembly of the catalytically competent state should occur during the second and third stages. To determine the nature of the processes taking place at these stages, conformational alterations of DNA have been recorded [35,92,93].

$$\mathrm{E + DHU} \underset{k_{-1}}{\overset{k_1}{\rightleftharpoons}} \mathrm{(E{\bullet}DHU)_1} \underset{k_{-2}}{\overset{k_2}{\rightleftharpoons}} \mathrm{(E{\bullet}DHU)_2} \underset{k_{-3}}{\overset{k_3}{\rightleftharpoons}} \mathrm{(E{\bullet}DHU)_3} \xrightarrow{k_{cat}} \mathrm{E{\bullet}P} \overset{K_p}{\rightleftharpoons} \mathrm{E + P}$$

Scheme 2. Kinetic mechanism of interaction between Nei and DHU-containing DNA substrate.

Examination of the structure of the active site suggests (Figure 16c) that the base located on the 5′ side of the damaged nucleotide is close to residue Leu70 and that the base situated opposite the damaged nucleotide engages in contacts with Gln69 and Tyr71 [35]. Therefore, duplexes containing a fluorescent dye on the 5′ side (**X-DHU/G$_{12}$**, X = aPu, C^{Py}, or 3HC) or opposite (**DHU/N$_{12}$**, N = aPu, C^{Py}, 3HC, or tC^{O}) to damaged base DHU have been used as promising substrates.

E is Nei; DHU is a DHU-containing DNA substrate; $(E{\bullet}DHU)_n$ are various enzyme–substrate complexes arising during the recognition of 5,6-dihydrouracil; E•P is the complex of E with reaction product P; k_i and k_{-i} are rate constants of the forward and reverse reactions of the individual steps.

This screening of fluorophores has revealed that aPu is not sensitive to the processes happening at the stages of complexation with the enzyme. It has been demonstrated that in the model system **X-DHU/G$_{12}$**, C^{Py} and 3HC lead to a complete loss of the catalytic activity of the enzyme. Consequently, we have employed the model system **DHU/N$_{12}$**, which has a much smaller effect on the catalytic activity of the enzyme. For all fluorophores (except for aPu, for which no changes have been detectable; Figure 17), concentration series of kinetic curves have been generated, and kinetic schemes and rate constants have been determined. Figure 17 presents examples of kinetic curves constructed with various fluorophores in the model system **DHU/N$_{12}$**.

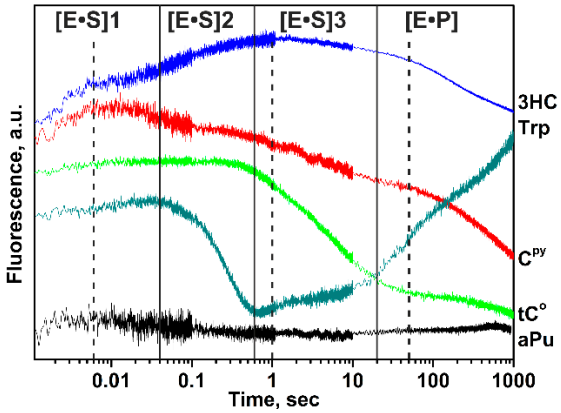

Figure 17. Interaction of Nei with various DHU-containing substrates carrying fluorescent base analogs aPu, C^{py}, tC^{O}, or 3HC opposite the DHU base. Vertical lines denote the time ranges of conformational changes in the enzyme that correspond to the kinetic stages in Scheme 2.

Registration of the fluorescence of Trp and of fluorophores in DNA has helped to uncover the coupled conformational dynamics of the enzyme and of DNA during the enzymatic process and to detail the nature of the stages of lesion recognition. The initial increase in fluorescence intensity of Trp and the initial rise of 3HC fluorescence intensity before time point 6 ms probably reflect the rapid "closure" of the N- and C-terminal domains of the enzyme during the appearance of the initial nonspecific complex. A comparison of the kinetic curves suggests that during the first change in Trp fluorescence intensity (up to time point 0.6 s), two conformational changes in DNA occur that can be registered by means of 3HC: a plateau from 0.006 to 0.02 s and a growth of intensity until 1.0 s. These phases of fluorescence kinetics of 3HC may mean the bending of the DNA helix, the eversion of the DHU base from the helix, and the subsequent intercalation of amino acid residues Gln69, Leu70, and Tyr71 into the DNA helix because these processes increase the hydrophobicity of the surroundings of the 3HC residue. The next rise in Trp fluorescence intensity (in the time interval from 1 to 10 s) leads to only a slight change in the fluorescence of 3HC. Within this period, the structure of the active site gets finely adjusted, which is necessary to achieve a catalytically competent state. The last change in fluorescence intensities of Trp and 3HC at time points after 10 s is the result of catalytic steps and dissociation of the enzyme–product complex, which afford a more hydrated environment for 3HC in the DNA product.

Several mutant versions of the enzyme have been used to determine the functions of various amino acid residues and to further clarify the nature of the specific steps of DNA binding. For the substitution, residues Leu70 and Tyr71, which get intercalated into the duplex, have been chosen, as well as residues Phe121, Phe230, and Pro253 (located in the DNA-binding site) and residue Glu2 (required for the catalytic reaction). Nei mutants

containing substitutions Glu2Gln, Leu70Ser, Leu70Trp, Tyr71Trp, Phe121Trp, Phe230Trp, or Pro253Trp have been generated by site-directed mutagenesis. Testing of the relative activity of the mutant enzymes has shown that the replacement of Glu2 or Leu70 causes a large loss of catalytic activity (Figure 18a). Changes in Trp fluorescence intensity, which characterize conformational rearrangements of the enzyme, have been documented during the interaction of each mutant with substrate **DHU/G$_{12}$** or **AP/G$_{12}$** (Figure 18b,c). Substitutions of Glu2 and Leu70, which eliminate the enzymatic activity, also lead to the almost complete disappearance of all changes in Trp fluorescence intensity. This finding indicates that the amplitude of changes in Trp fluorescence intensity reflects the course of the catalytic stages of the enzymatic process.

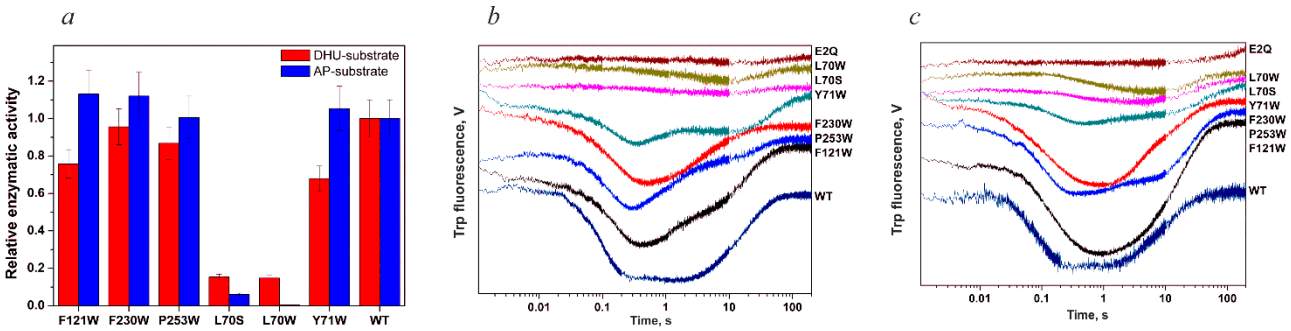

Figure 18. (**a**) Relative activity of wild-type Nei and mutants of the enzyme. Experimental kinetic curves describing conformational changes of the enzyme during the interaction of wild-type Nei or one of its mutants with (**b**) substrate **DHU/G$_{12}$** or (**c**) substrate **AP/G$_{12}$**.

Among the mutants Nei Tyr71Trp, Nei Phe121Trp, Nei Phe230Trp, and Nei Pro253Trp, which retain the enzymatic activity, the behaviors of Trp fluorescence intensity differ in the initial section of the kinetic curves up to 5 s, which characterizes the stages of damage recognition and assembly of the catalytic complex. Such differences from the shape of the curve of the wild-type enzyme imply the contribution of a new Trp residue to the fluorescence intensity. Furthermore, these differences allow us to conclude that there are conformational alterations in the enzyme in the region of this particular amino acid residue and to identify the time point and stage in the mechanism at which this amino acid gets involved. To calculate the rate constants, concentration series of kinetic curves have been obtained for each mutant (Table 5).

The weight of evidence describing the conformational alterations of the enzyme and of DNA substrates as well as mutational analysis has helped us to propose a molecular-kinetic mechanism of damage recognition by the Nei enzyme, where step 1 corresponds to the rapid initial binding of DNA and the formation of the nonspecific enzyme–substrate complex, in which the N- and C-terminal domains of the enzyme are in a closed position. In this complex, wedging of residue Leu70 into the duplex takes place, which is a key process in the search for a damaged DNA region. Step 2 includes the bending of the double helix at the site of the damaged base, the eversion of DHU from the duplex, and the intercalation of Tyr71 into DNA. This amino acid residue is necessary to stabilize the twisted conformation of the damaged nucleotide. In addition, at step 3, during the fine-tuning of the active site to achieve a catalytically competent state, Tyr71 gets involved too. At this step, contacts arise between Phe121 and the ribose-phosphate backbone of DNA. The formation of the catalytic complex leads to the hydrolysis of the *N*-glycosidic bond and subsequent reactions of β-elimination of 3′- and 5′-phosphate groups. The enzymatic cycle is completed by the dissociation of the enzyme–product complex.

Table 5. Rate and equilibrium constants characterizing the interaction of wild-type Nei or one of its mutants with substrate **DHU/G$_{12}$**.

Constants	L70S	L70W	Y71W	F121W	F230W	P253W	WT
k_1, $M^{-1}s^{-1}$	$(0.09 \pm 0.02) \times 10^6$	$(0.06 \pm 0.01) \times 10^6$	$(21 \pm 3) \times 10^6$	$(39 \pm 11) \times 10^6$	$(30 \pm 2) \times 10^6$	$(27 \pm 2) \times 10^6$	$(36 \pm 7) \times 10^6$
k_{-1}, s^{-1}	1 ± 0.1	0.4 ± 0.1	330 ± 30	120 ± 31	310 ± 45	310 ± 26	410 ± 20
K_1[a], M^{-1}	0.9×10^5	1.5×10^5	0.63×10^5	3×10^5	0.97×10^5	0.87×10^5	0.88×10^5
k_2, s^{-1}			16 ± 3	17 ± 4	21 ± 3	23 ± 3	27 ± 2
k_{-2}, s^{-1}			2.5 ± 0.1	0.55 ± 0.25	1.2 ± 0.1	0.8 ± 0.1	1.8 ± 0.3
K_2			6.4	31	17.5	28.7	15
k_3, s^{-1}			0.4 ± 0.1	0.58 ± 0.15	0.82 ± 0.04	1.0 ± 0.03	1.6 ± 0.1
k_{-3}, s^{-1}			1.1 ± 0.1	0.89 ± 0.14	0.66 ± 0.06	1.2 ± 0.1	1.5 ± 0.2
K_3			0.36	0.65	1.2	0.83	1.1
K_{ass}[b], M^{-1}			1.45×10^5	6×10^6	2×10^6	2×10^6	1.45×10^6
k_{cat}, s^{-1}	0.09 ± 0.01	0.08 ± 0.03	0.14 ± 0.03	0.26 ± 0.09	0.38 ± 0.01	0.4 ± 0.03	0.35 ± 0.02
K_p, M	$(1.0 \pm 0.2) \times 10^{-6}$	$(0.7 \pm 0.5) \times 10^{-6}$	$(0.4 \pm 0.1) \times 10^{-6}$	$(0.6 \pm 0.1) \times 10^{-6}$	$(0.6 \pm 0.2) \times 10^{-6}$	$(0.63 \pm 0.08) \times 10^{-6}$	$(0.7 \pm 0.1) \times 10^{-6}$

[a] $K_i = k_i/k_{-i}$, where i is the stage number, [b] $K_{ass} = K_1 \times K_2 \times K_3$.

4.2. Other Members of Structural Family H2tH: Fpg and NEIL1

Formamidopyrimidine DNA glycosylase Fpg has wide substrate specificity for oxidized nitrogenous bases, including oxoG [94,95]. This protein's molecule has a positively charged channel within which DNA binds. In the catalytic complex, the DNA is bent, the damaged base is flipped out of the duplex, and this free space is filled by residues Met73, Arg108, and Phe110 [96].

While working in this field, we have analyzed the accumulation of reaction products starting in the millisecond range by the "reaction interruption" (quench-flow) technique [97]. Our results indicate the existence of a stage of enzyme–substrate interaction after which the addition of a "quencher" (7 M urea) to the reaction mixture does not affect the attainment of the catalytic conformation; in other words, the dissociation of the enzyme–substrate complex proceeds more slowly than do intramolecular conformational rearrangements giving rise to the competent state and resulting in chemical stages. According to our results, this stage is the eversion of the damaged base.

Double electron–electron resonance spectroscopy has been utilized to determine the bending angle of DNA duplexes caused both by the damaged nucleotide itself and by the formation of a complex with Fpg [98,99]. It has been found that the presence of an F-site in the duplex leads to its bending by ~20°, whereas the nucleotide containing the damaged oxoG base does not affect the overall structure of the duplex. In addition, it has been demonstrated under equilibrium conditions that Fpg causes additional bending of the DNA duplex containing an F-site and induces the bending of intact DNA during the formation of the nonspecific complex.

Mass-spectrometric analysis of covalent reaction intermediates has been carried out [97], as performed for hOGG1. It has been shown that the stage of breakup of the covalent complex with a ribose residue is the rate-limiting stage of the entire enzymatic process.

Kinetic patterns of Fpg's catalysis at different temperatures have been studied during interactions with intact DNA or with one of the duplexes containing an F-site or oxoG [36]. Registration of DNA conformational changes has been performed by means of changes in fluorescence intensity of the C^{Py} residue located opposite a specific site. Via a similar approach, as in the case of hOGG1, concentration series of curves and rate constants have

been obtained for each temperature, enabling us to compute thermodynamic parameters of stages of the enzymatic process with the help of Van't Hoff's (Equation (9)) and Eyring's (Equation (10)) equations.

A combined analysis of the kinetic and thermodynamic data on the conformational transformations of the Fpg enzyme and DNA during their interaction has made it possible to propose the most probable interpretation of the nature of the conformational transitions occurring in the enzyme–substrate complex on the way to the catalytically competent state (Table 6). It should be pointed out that overall, the stages of DNA binding and damage recognition proceed at considerable enthalpy costs, but they are compensated by an increase in entropy due to the removal of water molecules from the contact area and to the formation of a tightly bound enzyme–substrate complex. In this context, dehydration of the protein–DNA interface begins at the stage of the emergence of the initial nonspecific complex.

Table 6. Thermodynamic parameters of the interaction of DNA glycosylase Fpg with ligand **G/C$^{Py}_{12}$** or **F/C$^{Py}_{12}$** or substrate **oxoG/C$^{Py}_{12}$**.

DNA	Parameter / Stage Number	ΔG°_{i298}, kcal/mol	ΔH°_{i}, kcal/mol	ΔS°_{i}, cal/(K·mol)	Process
G/C$^{Py}_{12}$	1	−7.0	−3.8 ± 0.9	10.9 ± 3.2	Nonspecific binding, local "melting" of segment of DNA duplex, dehydration
F/C$^{Py}_{12}$	1	−7.2	−4.0 ± 0.3	10.8 ± 1.0	Nonspecific binding, local "melting" of segment of DNA duplex, dehydration
	2	0.7	6.7 ± 0.3	20.3 ± 0.9	Kinking of DNA and intercalation of Fpg amino acid residues into duplex
	$\sum_{i=1}^{i=2}$	−6.5	2.7 ± 0.4	31.1 ± 1.3	
oxoG/C$^{Py}_{12}$	1	−7.0	−3.2 ± 0.4	12.7 ± 1.5	Nonspecific binding, local "melting" of segment of DNA duplex, dehydration
	2	0.4	0.3 ± 0.8	−0.3 ± 2.7	Insertion of "wedge" into DNA (amino acid residue Phe110) for discrimination between damaged and intact segments of DNA
	3	0.8	6.3 ± 1.7	18.4 ± 5.8	Kinking of DNA
	4	−1.5	−15.5 ± 3.9	−46.9 ± 13.5	Eversion of oxoG base into active site of Fpg concurrently with insertion of amino acid residues Arg108 and Met73 into resultant cavity in DNA helix
	5	−1.9	31.2 ± 5.5	111.1 ± 18.6	Final fine adjustment of active-site structure to attain catalytically competent state, dehydration of DNA grooves
	$\sum_{i=1}^{i=5}$	−9.2	19.1 ± 12.3	95.0 ± 42.1	
	6	19.6	6.0 ± 1.4	−45.5 ± 4.7	Transition state of catalytical chemical stage
	7	−7.0	−4.1 ± 0.3	9.6 ± 0.9	Formation of enzyme–product complex

The data are presented as the mean ± standard deviation. $\Delta\Delta G^{\circ}_{i298} = RT(\Delta K_i/K_i) \leq 0.1$ kcal/mol.

Human endonuclease VIII, NEIL1, is a eukaryotic member of this structural family [100,101]. A comparison of the currently known structure of the free NEIL1 enzyme [102,103] with the structures of complexes of Fpg or Nei with damaged DNA reveals a high level of structural homology. A comparison of the amino acid sequences of NEIL1, Fpg, and Nei also shows high homology among these enzymes. A fragment of sequences

(Figure 19) helps to see that the organization of amino acid residues that get intercalated into DNA after the eversion of a lesion is the same in NEIL1 as in Fpg, i.e., these residues are located at a distance from each other in the amino acid sequence, in contrast to Nei.

```
NEIL1    RGKELRLILSPLPGAQPQQEPLALVFRFGMSGSFQLVPREELPRHAHLRFYTAPPGPRLA   111
Fpg      RAKYLLLE---------LPEGWII-IHLGMSGSLRILPEELPPEKHDH--VDLVMSNGKV   102
Nei      RGKALLTH---------FSNDLTLYSHNQLYGVWRVVDTSEEPQTTRVLRVKLQTADKTI   101
         *.* *              :   :  :  : *  :::  .  *.          .

NEIL1    LCFVDIRRFGRWDLGGKW-----QPGRGPCVLQEYQQFRENVL--RNLADKAFDRPICEA   164
Fpg      LRYTDPRRFGAWLWTKELEGHNVLTHLGPEPLSDD--FNGEYLHQKCAK---KKTAIKPW   157
Nei      LLYSASD--IEMLRPEQLTTHPFLQRVGPDVLDPN--LTPEVVKERLLSPRFRNRQFAGL   157
         * :              :          **  *.    :  : :  :       .  :
```

Figure 19. A comparison of sequence fragments of NEIL1, Fpg, and Nei. Amino acid residues that get inserted into DNA are highlighted in red [104].

The high structural homology between NEIL1, Fpg, and Nei implies that during the formation of the catalytic complex, NEIL1 probably undergoes in a similar way the conformational rearrangements related to the recognition of the damaged nucleotide, then the bending of DNA, the inversion of the damaged base into the enzyme active site, and the intercalation of amino acid residues into the DNA. Accordingly, to register the mutual conformational changes of NEIL1 and DNA during their interaction, the same approach has been used as with Nei and Fpg [104]. For registration of the conformational changes in the enzyme by means of changes in Trp fluorescence intensity as DNA substrates, a series of duplexes have been employed that contain in the central part an intact nucleotide (duplex $\mathbf{G/C_{12}}$) or a modified nucleotide (duplex $\mathbf{X/G_{12}}$, where X = F-site, AP-site, or DHU). The kinetic curves obtained under the same conditions for the enzymes of this family have revealed major differences in the kinetics of changes in Trp fluorescence intensity [104]. That is, despite similar structural patterns of the formation of the catalytic complex and the high homology, the changes in Trp fluorescence intensity in each case are determined by individual features of the positioning of Trp residues in an enzyme's globule. Nonetheless, a common characteristic of all kinetic curves is a local minimum of Trp fluorescence intensity during the formation of the catalytic complex in the course of interaction with various "cleavable" DNA duplexes containing an AP-site or DHU. Additionally, DNA duplexes ($\mathbf{X^{FAM/BHQ1}/G_{17}}$, where X = C, F-site, AP-site, or DHU) containing the dyes FAM and BHQ1 at the 5′ ends of the oligonucleotides forming the duplex have been employed to record the DNA conformational changes. The stages of DNA bending and catalysis have been documented, kinetic schemes have been determined, and constants have been calculated [104]. The obtained results [104] with NEIL1 fit the general picture of DNA glycosylases as enzymes that initiate damage recognition through indirect readout, probing DNA for flexibility or other conformational response to the strain induced upon enzyme binding, and using direct contacts with the damaged base only at later stages of the reaction to confirm the presence of the lesion.

4.3. A General Model for the Recognition of DNA Damage by Enzymes of Structural Family H2tH

Summarizing the data on this class of enzymes, it can be said that the process of recognition of a damaged nucleotide is represented by a common model among the studied pro- and eukaryotic members of the family (Table 7). At the first stage, the initial nonspecific complex forms between an enzyme and a DNA substrate, accompanied by destabilization of the duplex and its local "melting". In the nonspecific complex, a "sensor" amino acid residue (Phe110 in Fpg, Leu70 in Nei, and Phe119 in NEIL1) is wedged between DNA bases, thus causing additional destabilization of the double helix. The wedging of the sensor into the duplex initiates the eversion of the damaged base into the active site of the enzyme. A comparison of the kinetic curves obtained with FRET substrates indicates that duplex bending and incorporation of the other residues of the triad into DNA (Met73 and Arg108 in Fpg, Gln69 and Tyr71 in Nei, and Met80 and Arg117 in NEIL1), which

stabilize the out-of-helix position of the lesion, proceed in a coordinated manner. At the last stage, the structure of the enzyme–substrate complex is fine-tuned to attain a catalytically competent state. According to the thermodynamic data obtained about Fpg, at this stage, the enzyme–substrate complex is compacted and water molecules are displaced from the contact area between the enzyme and the DNA substrate. Then, the chemical stages of the process take place, with subsequent dissociation of the enzyme–product complex.

Table 7. Key steps in damage recognition by enzymes of structural family H2tH.

	Nei (*E. coli*)	**Fpg (*E. coli*)**	**NEIL1**
Destabilization of double helix, local "melting"	+	+	+
Intercalation of "sensor"	Leu70	Phe110	Phe119
Eversion of damaged base and duplex bending	+	+	+
Intercalation of other amino acid residues	Gln69, Tyr71	Met78, Arg108	Met80, Arg117

5. Human AP Endonuclease APE1

Human AP endonuclease 1 is a Mg^{2+}-dependent enzyme and differs from DNA glycosylases both in structure and catalytic properties [105–107] (Figure 20). AP endonuclease processes intermediate DNA products generated by DNA glycosylases in the course of BER and cleaves an AP site, which is caused by spontaneous loss of a nitrogenous base [108,109]. It is generally accepted that the main function of AP endonucleases in the cell is the cleavage of DNA from the 5′ terminus of the AP site or the removal of 3′-end-blocking groups such as 3′-phospho-α,β-unsaturated aldehyde or 3′-terminal phosphate, thereby producing a 3′-hydroxyl group required for DNA synthesis by polymerase [110–112]. Data obtained over the last two decades clearly indicate that AP endonucleases can recognize as substrates not only an AP site but also various damaged nucleotides, for example, 5,6-dihydro-2′-deoxyuridine, the α-anomer of 2′-deoxyadenosine (αA), and several others [106,113–119]. In addition, these enzymes possess endoribonuclease [120–122], 3′-phosphodiesterase, 3′-phosphatase [112] and 3′-5′-exonuclease activities [32,123,124].

Notably, the functional class of AP endonucleases is comparable to the well-studied class of DNA glycosylases. Indeed, the mechanisms of recognition of a single-nucleotide lesion by DNA glycosylases have been comprehensively studied by structural, mutational, and kinetic approaches in the course of the last three decades. It has been revealed that DNA glycosylases from six structural families have different structures of the DNA-binding site and of the catalytically active site and distinct functional amino acid residues involved in specific recognition of a damaged nucleotide and in catalysis; however, almost all these enzymes have common features of interaction with damaged DNA [73,86,125,126]. These data have improved our understanding of how the recognition of single-nucleotide lesions occurs. For instance, all DNA glycosylases (with the exception of enzymes from the ALK family [127]) with currently available structures bend DNA and flip out the damaged nucleotide and/or complementary nucleotide from the DNA double helix. As a general rule, the damaged nucleotide is placed in the active-site pocket, where its final verification takes place. Some amino acid residues of the enzyme are inserted into the formed void in the DNA duplex (void-filling amino acid residues) and can act either as a specific 'wedge' sensing the lesion and pushing out the damaged nucleotide or as non-specific anchor residues that stabilize the extra-helical position of the damaged nucleotide [44,72,93,100,128–132].

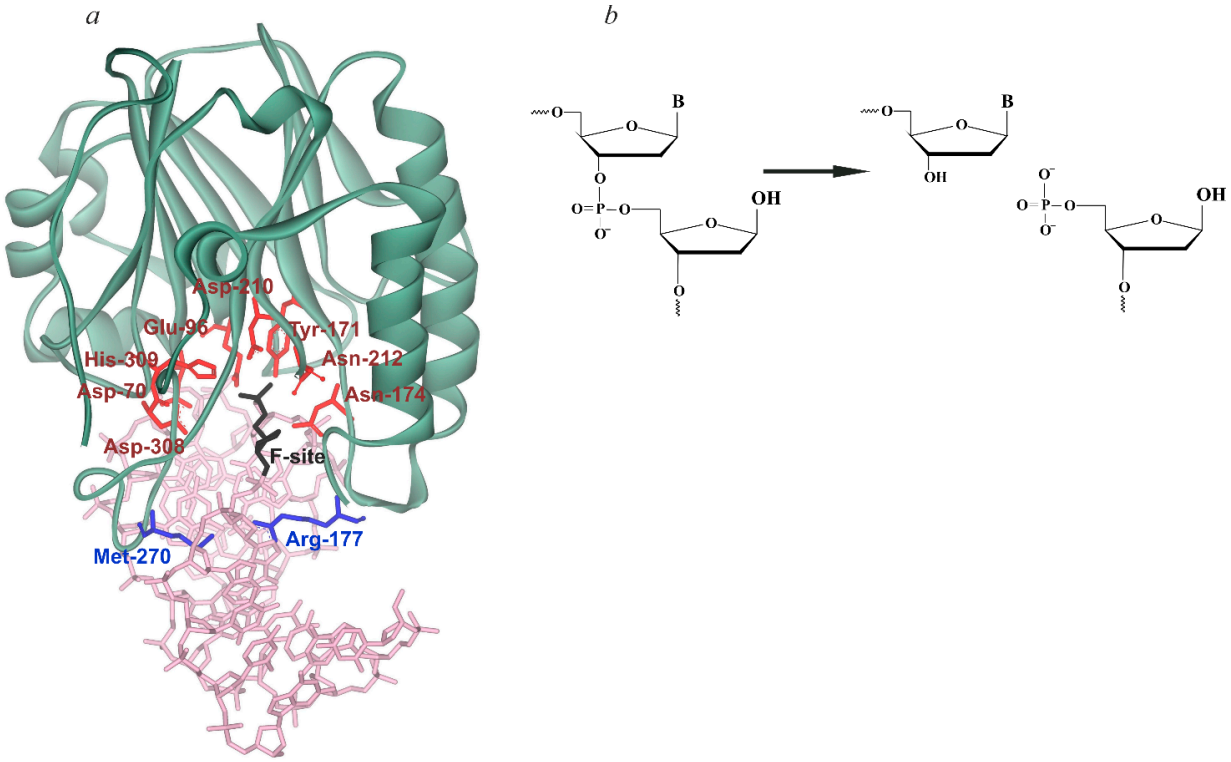

Figure 20. (**a**) Structure of the complex of AP endonuclease APE1 with an F-site-containing substrate (F-substrate) (PDB ID 1DE8). (**b**) APE1-catalyzed hydrolysis of the phosphodiester bond on the 5′ side of an AP-site.

According to the structural data [133,134], this strategy of damage recognition is suitable for AP endonucleases. An analysis of the crystal structures of the free enzyme APE1 [135–137] and of its complexes with DNA [133,138,139] suggests that amino acid residues of the enzyme interact predominantly with one strand of the duplex. Human AP endonuclease APE1 in complex with an abasic DNA causes a bending of the chain at an angle of ~35°, the eversion of the damaged nucleotide, and its insertion into the active site. There are also two 'wedging' amino acid residues, Arg177 and Met270, inserted into the DNA helix after the abasic-site eversion. In this complex, the nucleotide located opposite the lesion retains stacking with neighboring bases in the DNA duplex [138].

The kinetic mechanism of conformational changes in APE1 and in abasic DNA molecules in the course of their interaction was studied by recording the intrinsic tryptophan fluorescence of the enzyme [139,140] and the 2-aminopurine fluorescence in the DNA [141]. To elucidate the mechanism of substrate specificity of AP endonucleases, an interaction of enzymes with DNA was analyzed by double electron–electron resonance (DEER, also known as pulsed electron–electron double resonance, PELDOR) spectroscopy [56,142,143] and molecular dynamic simulations [142,144,145], as well as by real-time fluorescent detection of conformational rearrangements of the enzyme and DNA during their interaction [32,33,55,146–151]. The influence of singly (Figure 21a) and doubly (Figure 21b) charged metal ions [152] on APE1's DNA binding and catalysis has been determined. It was shown that the first step of substrate binding (corresponding to the formation of a primary enzyme–substrate complex) does not depend on the concentration (0.05–5.0 mM) or the nature of divalent metal ions. In contrast, the initial DNA binding efficiency significantly decreased at a high concentration (5–250 mM) of monovalent K^+ ions, indicating the involvement of electrostatic interactions in this stage.

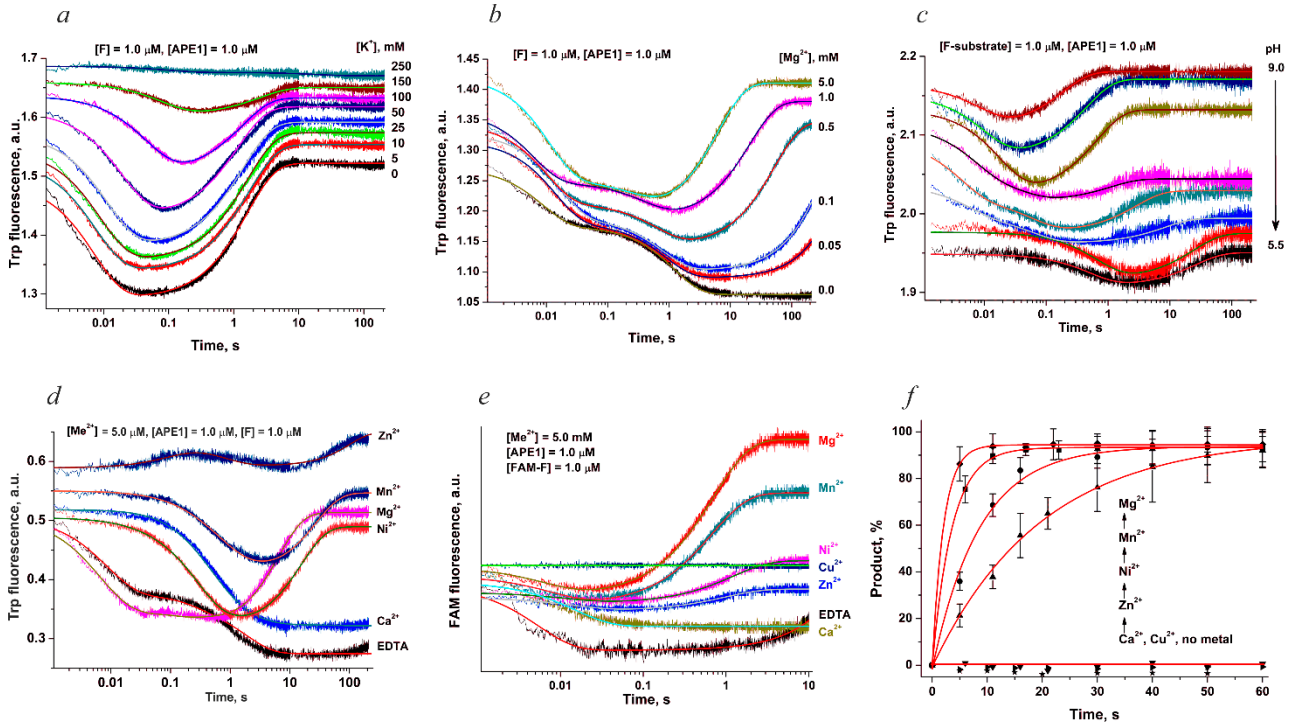

Figure 21. The influence of ions K^+ (**a**) and Mg^{2+} (**b**) and of pH (**c**) on APE1 activity. Effects of ions on the activity of APE1 toward F-substrate. The impact of the nature of divalent metal ions on the conformational alterations of APE1 (**d**) and of the DNA substrate (**e**) and on the rate of accumulation of reaction products (**f**).

The kinetics of conformational changes of the enzyme and of DNA substrate molecules were studied during the recognition and cleavage of the abasic site in the pH range from 5.5 to 9.0 using stopped-flow fluorescence techniques (Figure 21c) [147]. The activity of APE1 increased with an increase in pH because of the acceleration of the rates of catalytic complex formation and the catalytic reaction. A molecular dynamics simulation uncovered a significant increase in the p*K*a of His-309 located in the active site of the enzyme. This finding revealed that the observed enhancement of enzymatic activity with pH could be associated with the deprotonation of not only Tyr-171 but also His-309. The obtained data allowed us to hypothesize that the ionized state of these residues could be a molecular switch between the alternative catalytic mechanisms, which involve different functionalities of these residues throughout the reaction.

Additionally, using Trp fluorescence (Figure 21d), a FRET signal (Figure 21e), and direct product detection (Figure 21f), it has been shown [152] that the nature of the doubly charged metal also affects these processes. It has been demonstrated that the rate of formation of the initial complex does not depend on the concentration of doubly charged metals; however, they accelerate the second stage of DNA binding. In these experiments, the absence of doubly charged ions or the presence of Cu^{2+} or Ca^{2+} completely inactivates the enzyme, and the efficiency of other metal ions for the hydrolysis of the phosphodiester bond increases in the series $Zn^{2+} < Ni^{2+} < Mn^{2+} < Mg^{2+}$.

To clarify the nature of the processes occurring during the successive stages of F-site recognition in a DNA substrate, of catalysis, and of dissociation of the enzyme–product complex, a stepwise thermodynamic analysis of the interaction of APE1 with F-substrate has been performed [153]. Examination of the kinetic curves of changes in protein fluorescence intensity has revealed that the minimal kinetic mechanism of the interaction of APE1 with F-substrate includes two-stage equilibrium binding, irreversible formation of the enzyme–product complex, and equilibrium dissociation of this complex (Scheme 3).

$$E + S \underset{k_{-1}}{\overset{k_1}{\rightleftarrows}} (E\bullet S)_1 \underset{k_{-2}}{\overset{k_2}{\rightleftarrows}} (E\bullet S)_2 \xrightarrow{k_{cat}} E\bullet P \overset{K_P}{\rightleftarrows} E + P$$

Scheme 3. Kinetic mechanism of interaction between APE1 and DNA substrate, containing F-site.

E is the enzyme, S is a DNA substrate, $(E\bullet S)_1$ and $(E\bullet S)_2$ are enzyme–substrate complexes, P is a substrate conversion product, E•P is the enzyme–product complex, k_i and k_{-i} are rate constants of forward and reverse reactions of the equilibrium stages, k_3 is the rate constant of the catalytic stage, and K_p is the equilibrium dissociation constant of the E•P complex.

According to the findings [153], the formation of the initial enzyme–substrate complex (the first stage in Scheme 3) involves a positive change in standard enthalpy (14.3 kcal/mol) and a positive change in entropy [79.0 cal/(mol·K)]. Given that the increase in entropy during the interaction of DNA-binding proteins with DNA is due either to the desolvation of polar groups at the protein–DNA interface or to the displacement of highly ordered "crystalline" water molecules from DNA grooves, it can be concluded that at this stage, bonds appear between amino acid residues of a DNA-binding site and the DNA duplex. Among them, we can highlight the interaction between phosphate groups of the DNA duplex on the 5′ and 3′ sides of the F-site and residues Arg73, Ala74, Lys78, Trp280, Asn222, Asn226, and Asn229 (Figure 20a). Furthermore, at this moment, intercalation of residue Arg177 probably occurs into the DNA duplex on the side of the major groove, as does the formation of a hydrogen bond with the phosphate group located on the 3′ side of the F-site. Residue Met270 gets intercalated into the DNA duplex on the minor-groove side and can also displace "crystalline" water.

Obtained data [153] allow us to suggest that the second stage of the interaction of APE1 with F-substrate—a specific rearrangement of complex $(E\bullet S)_1$—features a negative change in both enthalpy ($\Delta H^\circ_2 = -6.8$ kcal/mol) and entropy [−24.6 cal/(mol·K)]. A negative value of ΔH°_2 indicates the stabilization of the complex during the formation of new, energetically favorable bonds between the interacting atoms, whereas a negative value of ΔS°_2 denotes an increase in the complex's rigidity, i.e., a reduction in internal degrees of freedom. These results indicate that this step includes the process of F-site inversion into the active site of the enzyme and stabilization of this state by residues Arg177 and Met270, which get inserted into the major and minor grooves of DNA, respectively. Additionally, at this point, there is likely the formation of bonds between a phosphate group located in the 5′ direction from the F-site, residues Asn174, Asn212, and His309, and the Mg^{2+} ion located in the enzyme active site.

For the catalytic stage, we have calculated changes in enthalpy ($\Delta H^{\neq}$) and entropy ($\Delta S^{\neq}$) of activation of transition complex formation. The enthalpy of activation proved to be 12.2 kcal/mol. This value refers to the stage of hydrolysis of the phosphodiester bond by the APE1 enzyme and is in the range of 6.0–18.6 kcal/mol for the catalytic stages of reactions of *N*-glycosidic bond cleavage and β-elimination of phosphate groups carried out by DNA glycosylases Fpg and hOGG1.

6. Conclusions

Within this review, studies on the application of a comprehensive methodology for investigation into the mechanisms of DNA damage recognition by base excision repair enzymes on the basis of kinetic, thermodynamic, and mutational assays of conformational alterations in enzymes and DNA were described. *The kinetic analysis* of conformational changes in enzymes and DNA during the assembly and transformation of enzyme–substrate complexes has involved methods of pre-steady-state kinetics because damage recognition processes are fast. In some cases, conformational changes in the DNA helix were proven by PELDOR spectroscopy. *To correlate conformational changes in DNA with interactions of certain residues* during the formation of specific enzyme–substrate complexes, the method of a stepwise increase in ligand complexity has been used. *The*

thermodynamic analysis has been based on research into enzymatic processes using the stopped-flow method with fluorimetric detection at various temperatures. *The mutational analysis* has been based on the use of mutant versions of enzymes containing a substitution of amino acid residues present in the active site of the enzyme and at sites of binding to a substrate. *The mass-spectrometric analysis* of intermediates of the enzymatic process catalyzed by enzymes Fpg and hOGG1 has confirmed that the rate-limiting step is the reaction of β-elimination of the phosphate group. Moreover, the regeneration of DNA glycosylase Fpg from the complex with a ribose residue is slow and can also limit the rate of the enzymatic process in a steady-state reaction. Taken together, the results obtained by all these approaches and the characterization of conformational changes in both enzymes or their mutants and model DNA duplexes containing modifications of varying degrees of specificity to the enzyme and various fluorophores have allowed the *determination of detailed molecular-kinetic mechanisms underlying the recognition of specific sites in DNA, the formation of catalytically competent complexes, and the course of chemical-reaction steps*.

Still, the stopped-flow method has restricted applicability, but it has become more widely known and appreciated, and consequently, the limits of the kinetics technique are continually pushing. Indeed, the methodology developed during the described research can be extended to studies not only on DNA-processing enzymes but also on protein–protein interactions as well as interactions of enzymes with low-molecular-weight substrates (e.g., peptides, amino acids, and nucleotides) or small-molecule inhibitors or activators of enzymatic processes.

Although fluorescence does not provide detailed structural information, its utility in defining structural dynamics and molecular interactions places it at the top of the list of possible methods that could be applied to address such questions. Clearly, fast kinetic methods, like any technique, should not be used alone. Rather, its lack of capabilities on the structural level should be compensated for by the use of complementary approaches. The modern level of scientific research makes it possible to combine the information of the crystal structure "photo" at the atomic level with a full-length "film" of conformational dynamics in the process of enzyme-substrate interaction in real time, recorded using sensitive fluorescent dyes. In the mind of the author, stopped-flow technology with fluorescence detection, given its many advantages, will no doubt continue to be applied in the fields of biophysics, biophysical chemistry, and molecular biology for a very long time.

Funding: This work was supported by Russian Science Foundation grant No. 23-44-00064. Partial support by a Russian-State-funded budget project No. 121031300041-4 for the routine maintenance of the equipment used is also acknowledged.

Institutional Review Board Statement: Not applicable.

Informed Consent Statement: Not applicable.

Data Availability Statement: Data are available upon request to N.A.K. Tel. +7-383-363-5174, E-mail: nikita.kuznetsov@niboch.nsc.ru.

Acknowledgments: Dedicated to Olga S. Fedorova, my teacher, outstanding scientist in the field of physical and chemical biology, and initiator of kinetic studies of many enzymes, including those described in this review.

Conflicts of Interest: The author declare no conflict of interest.

Glossary

aPu	2-aminopurine;
AP-site	apurinic/apyrimidinic site;
APE1	human apurinic/apyrimidinic endonuclease 1;
BER	base excision repair;
BHQ1	black hole quencher 1;
C^{Py}	pyrrolocytosine;
DHU	5,6-dihydrouracil;
F-site	(2*R*,3*S*)−2-(hydroxymethyl)−3-hydroxytetrahydrofuran residue (AP-site analogue);
FAM	6-carboxyfluorescein;
Fpg	formamidopyrimidine DNA glycosylase from *Escherichia coli*;
FRET	Forster resonance energy transfer;
HhH-GPD	structural family of DNA glycosylases containing the helix-hairpin-helix motif and a region enriched with glycine and proline residues (Gly/Pro loop) and the aspartate residue (D);
H2tH	structural family of DNA glycosylases containing helix-two turn-helix motif;
hOGG1	human 8-oxoguanine DNA glycosylase;
MutY	adenine-DNA glycosylase from *Escherichia coli*;
MBD4	human methyl-CpG-binding domain 4;
Nth	endonuclease III from *Escherichia coli*;
Nei	endonuclease VIII from *Escherichia coli*;
NEIL1	human endonuclease VIII;
oxoG	8-oxoguanine;
PDB ID	Protein Data Bank Identification number;
tC^{O}	1,3-diaza-2-oxophenoxazine;
WT	wild type enzyme;
PAGE	polyacrylamide gel electrophoresis;
3HC	3-hydroxychromone.

References

1. Friedberg, E.C.; Walker, G.C.; Siede, W.; Wood, R.D.; Schultz, R.A.; Ellenberger, T. *DNA Repair and Mutagenesis*; ASM Press: Washington, DC, USA, 2006.
2. Fromme, J.C.; Verdine, G.L. Base Excision Repair. *Adv. Protein Chem.* **2004**, *69*, 1–41. [CrossRef]
3. David, S.S.; O'Shea, V.L.; Kundu, S. Base-Excision Repair of Oxidative DNA Damage. *Nature* **2007**, *447*, 941–950. [CrossRef]
4. Wallace, S.S. Base Excision Repair: A Critical Player in Many Games. *DNA Repair* **2014**, *19*, 14–26. [CrossRef] [PubMed]
5. Zharkov, D.O. Base Excision DNA Repair. *Cell. Mol. Life Sci.* **2008**, *65*, 1544–1565. [CrossRef] [PubMed]
6. Kladova, O.A.; Kuznetsov, N.A.; Fedorova, O.S. Initial Stages of DNA Base Excision Repair in Nucleosomes. *Mol. Biol.* **2021**, *55*, 167–181. [CrossRef]
7. Krokan, H.E.; Bjørås, M. Base Excision Repair. *Cold Spring Harb. Perspect. Biol.* **2013**, *5*, a012583. [CrossRef]
8. Robertson, A.B.; Klungland, A.; Rognes, T.; Leiros, I. DNA Repair in Mammalian Cells: Base Excision Repair: The Long and Short of It. *Cell. Mol. Life Sci.* **2009**, *66*, 981–993. [CrossRef]
9. Gros, L.; Saparbaev, M.K.; Laval, J. Enzymology of the Repair of Free Radicals-Induced DNA Damage. *Oncogene* **2002**, *21*, 8905–8925. [CrossRef]
10. Tudek, B. Base Excision Repair Modulation as a Risk Factor for Human Cancers. *Mol. Asp. Med.* **2007**, *28*, 258–275. [CrossRef]
11. Wallace, S.S.; Murphy, D.L.; Sweasy, J.B. Base Excision Repair and Cancer. *Cancer Lett.* **2012**, *327*, 73–89. [CrossRef]
12. Marsden, C.G.; Dragon, J.A.; Wallace, S.S.; Sweasy, J.B. Base Excision Repair Variants in Cancer. *Methods Enzym.* **2017**, *591*, 119–157. [CrossRef]
13. Chan, K.K.L.; Zhang, Q.M.; Dianov, G.L. Base Excision Repair Fidelity in Normal and Cancer Cells. *Mutagenesis* **2006**, *21*, 173–178. [CrossRef]
14. Maynard, S.; Schurman, S.H.; Harboe, C.; de Souza-Pinto, N.C.; Bohr, V.A. Base Excision Repair of Oxidative DNA Damage and Association with Cancer and Aging. *Carcinogenesis* **2009**, *30*, 2–10. [CrossRef] [PubMed]
15. Kladova, O.A.; Fedorova, O.S.; Kuznetsov, N.A. The Role of Natural Polymorphic Variants of DNA Polymerase β in DNA Repair. *Int. J. Mol. Sci.* **2022**, *23*, 2390. [CrossRef] [PubMed]
16. Helleday, T.; Eshtad, S.; Nik-Zainal, S. Mechanisms Underlying Mutational Signatures in Human Cancers. *Nat. Rev. Genet.* **2014**, *15*, 585–598. [CrossRef]
17. Helleday, T.; Petermann, E.; Lundin, C.; Hodgson, B.; Sharma, R.A. DNA Repair Pathways as Targets for Cancer Therapy. *Nat. Rev. Cancer* **2008**, *8*, 193–204. [CrossRef] [PubMed]

18. Lakowicz, J.R. *Principles of Fluorescence Spectroscopy*, 3rd ed.; Springer: New York, NY, USA, 2006.
19. Carpenter, M.L.; Oliver, A.W.; Kneale, G.G. Analysis of DNA-Protein Interactions by Intrinsic Fluorescence. *Methods Mol. Biol.* **2001**, *148*, 491–502. [CrossRef] [PubMed]
20. Wong, I.; Lundquist, A.J.; Bernards, A.S.; Mosbaugh, D.W. Presteady-State Analysis of a Single Catalytic Turnover by *Escherichia coli* Uracil-DNA Glycosylase Reveals a "Pinch-Pull-Push" Mechanism. *J. Biol. Chem.* **2002**, *277*, 19424–19432. [CrossRef] [PubMed]
21. Dunlap, C.A.; Tsai, M.D. Use of 2-Aminopurine and Tryptophan Fluorescence as Probes in Kinetic Analyses of DNA Polymerase β. *Biochemistry* **2002**, *41*, 11226–11235. [CrossRef]
22. Cherepanov, A.V.; de Vries, S. Binding of Nucleotides by T4 DNA Ligase and T4 RNA Ligase: Optical Absorbance and Fluorescence Studies. *Biophys. J.* **2001**, *81*, 3545–3559. [CrossRef]
23. Wilhelmsson, L.M. Fluorescent Nucleic Acid Base Analogues. *Q. Rev. Biophys.* **2010**, *43*, 159–183. [CrossRef] [PubMed]
24. Sinkeldam, R.W.; Greco, N.J.; Tor, Y. Fluorescent Analogs of Biomolecular Building Blocks: Design, Properties, and Applications. *Chem. Rev.* **2010**, *110*, 2579–2619. [CrossRef] [PubMed]
25. Kim, K.T.; Kim, H.W.; Moon, D.; Rhee, Y.M.; Kim, B.H. (DNS)C: A Fluorescent, Environmentally Sensitive Cytidine Derivative for the Direct Detection of GGG Triad Sequences. *Org. Biomol. Chem.* **2013**, *11*, 5605–5614. [CrossRef]
26. Suzuki, A.; Takahashi, N.; Okada, Y.; Saito, I.; Nemoto, N.; Saito, Y. Naphthalene-Based Environmentally Sensitive Fluorescent 8-Substituted 2′-Deoxyadenosines: Application to DNA Detection. *Bioorg. Med. Chem. Lett.* **2013**, *23*, 886–892. [CrossRef] [PubMed]
27. Pawar, M.G.; Nuthanakanti, A.; Srivatsan, S.G. Heavy Atom Containing Fluorescent Ribonucleoside Analog Probe for the Fluorescence Detection of RNA-Ligand Binding. *Bioconjug. Chem.* **2013**, *24*, 1367–1377. [CrossRef]
28. Pawar, M.G.; Srivatsan, S.G. Environment-Responsive Fluorescent Nucleoside Analogue Probe for Studying Oligonucleotide Dynamics in a Model Cell-like Compartment. *J. Phys. Chem. B* **2013**, *117*, 14273–14282. [CrossRef]
29. Purohit, V.; Grindley, N.D.F.; Joyce, C.M. Use of 2-Aminopurine Fluorescence to Examine Conformational Changes during Nucleotide Incorporation by DNA Polymerase I (Klenow Fragment). *Biochemistry* **2003**, *42*, 10200–10211. [CrossRef]
30. Mandal, S.S.; Fidalgo da Silva, E.; Reha-Krantz, L.J. Using 2-Aminopurine Fluorescence to Detect Base Unstacking in the Template Strand during Nucleotide Incorporation by the Bacteriophage T4 DNA Polymerase. *Biochemistry* **2002**, *41*, 4399–4406. [CrossRef]
31. Kuznetsov, N.A.; Koval, V.V.; Zharkov, D.O.; Vorobjev, Y.N.; Nevinsky, G.A.; Douglas, K.T.; Fedorova, O.S. Pre-Steady-State Kinetic Study of Substrate Specificity of *Escherichia coli* Formamidopyrimidine-DNA Glycosylase. *Biochemistry* **2007**, *46*, 424–435. [CrossRef]
32. Kuznetsova, A.A.; Fedorova, O.S.; Kuznetsov, N.A. Kinetic Features of 3′-5′ Exonuclease Activity of Human AP-Endonuclease APE1. *Molecules* **2018**, *23*, 2101. [CrossRef]
33. Davletgildeeva, A.T.; Kuznetsova, A.A.; Fedorova, O.S.; Kuznetsov, N.A. Activity of Human Apurinic/Apyrimidinic Endonuclease APE1 toward Damaged DNA and Native RNA with Non-Canonical Structures. *Front. Cell Dev. Biol.* **2020**, *8*, 590848. [CrossRef]
34. Zang, H.; Fang, Q.; Pegg, A.E.; Guengerich, F.P. Kinetic Analysis of Steps in the Repair of Damaged DNA by Human O6-Alkylguanine-DNA Alkyltransferase. *J. Biol. Chem.* **2005**, *280*, 30873–30881. [CrossRef]
35. Kuznetsova, A.A.; Kuznetsov, N.A.; Vorobjev, Y.N.; Barthes, N.P.F.; Michel, B.Y.; Burger, A.; Fedorova, O.S. New Environment-Sensitive Multichannel DNA Fluorescent Label for Investigation of the Protein-DNA Interactions. *PLoS ONE* **2014**, *9*, e100007. [CrossRef]
36. Kuznetsov, N.A.N.A.; Vorobjev, Y.N.Y.N.; Krasnoperov, L.N.L.N.; Fedorova, O.S.O.S. Thermodynamics of the Multi-Stage DNA Lesion Recognition and Repair by Formamidopyrimidine-DNA Glycosylase Using Pyrrolocytosine Fluorescence—Stopped-Flow Pre-Steady-State Kinetics. *Nucleic Acids Res.* **2012**, *40*, 7384–7392. [CrossRef]
37. Yang, K.; Stanley, R.J. The Extent of DNA Deformation in DNA Photolyase-Substrate Complexes: A Solution State Fluorescence Study. *Photochem. Photobiol.* **2008**, *84*, 741–749. [CrossRef] [PubMed]
38. Sandin, P.; Borjesson, K.; Li, H.; Martensson, J.; Brown, T.; Wilhelmsson, L.M.; Albinsson, B. Characterization and Use of an Unprecedentedly Bright and Structurally Non-Perturbing Fluorescent DNA Base Analogue. *Nucleic Acids Res.* **2008**, *36*, 157–167. [CrossRef]
39. Borjesson, K.; Sandin, P.; Wilhelmsson, L.M. Nucleic Acid Structure and Sequence Probing Using Fluorescent Base Analogue TC(O). *Biophys. Chem.* **2009**, *139*, 24–28. [CrossRef]
40. Stengel, G.; Purse, B.W.; Wilhelmsson, L.M.; Urban, M.; Kuchta, R.D. Ambivalent Incorporation of the Fluorescent Cytosine Analogues TC and TCo by Human DNA Polymerase Alpha and Klenow Fragment. *Biochemistry* **2009**, *48*, 7547–7555. [CrossRef] [PubMed]
41. Stengel, G.; Urban, M.; Purse, B.W.; Kuchta, R.D. High Density Labeling of Polymerase Chain Reaction Products with the Fluorescent Base Analogue TCo. *Anal. Chem.* **2009**, *81*, 9079–9085. [CrossRef]
42. Rodgers, B.J.; Elsharif, N.A.; Vashisht, N.; Mingus, M.M.; Mulvahill, M.A.; Stengel, G.; Kuchta, R.D.; Purse, B.W. Functionalized Tricyclic Cytosine Analogues Provide Nucleoside Fluorophores with Improved Photophysical Properties and a Range of Solvent Sensitivities. *Chemistry* **2014**, *20*, 2010–2015. [CrossRef]
43. Sandin, P.; Stengel, G.; Ljungdahl, T.; Borjesson, K.; Macao, B.; Wilhelmsson, L.M. Highly Efficient Incorporation of the Fluorescent Nucleotide Analogs TC and TCO by Klenow Fragment. *Nucleic Acids Res.* **2009**, *37*, 3924–3933. [CrossRef]

44. Kuznetsov, N.A.; Kladova, O.A.; Kuznetsova, A.A.; Ishchenko, A.A.; Saparbaev, M.K.; Zharkov, D.O.; Fedorova, O.S. Conformational Dynamics of DNA Repair by *Escherichia coli* Endonuclease III. *J. Biol. Chem.* **2015**, *290*, 14338–14349. [CrossRef] [PubMed]
45. Rist, M.J.; Marino, J.P. Fluorescent Nucleotide Base Analogs as Probes of Nucleic Acid Structure, Dynamics and Interactions. *Curr. Org. Chem.* **2002**, *6*, 775–793. [CrossRef]
46. Berry, D.A.; Jung, K.Y.; Wise, D.S.; Sercel, A.D.; Pearson, W.H.; Mackie, H.; Randolph, J.B.; Somers, R.L. Pyrrolo-DC and Pyrrolo-C: Fluorescent Analogs of Cytidine and 2′-Deoxycytidine for the Study of Oligonucleotides. *Tetrahedron Lett.* **2004**, *45*, 2457–2461. [CrossRef]
47. Vasilyeva, S.V.; Kuznetsov, N.A.; Kuznetsova, A.S.; Khalyavina, J.G.; Tropina, D.A.; Lavrikova, T.I.; Kargina, O.I.; Gornostaev, L.M. DNA Fluorescent Labeling with Naphtho[1,2,3-Cd]Indol-6(2H)-One for Investigation of Protein-DNA Interactions. *Bioorg. Chem.* **2017**, *72*, 268–272. [CrossRef]
48. Dziuba, D.; Postupalenko, V.Y.; Spadafora, M.; Klymchenko, A.S.; Guerineau, V.; Mely, Y.; Benhida, R.; Burger, A. A Universal Nucleoside with Strong Two-Band Switchable Fluorescence and Sensitivity to the Environment for Investigating DNA Interactions. *J. Am. Chem. Soc.* **2012**, *134*, 10209–10213. [CrossRef]
49. Kuznetsova, A.A.; Kladova, O.A.; Barthes, N.P.F.; Michel, B.Y.; Burger, A.; Fedorova, O.S.; Kuznetsov, N.A. Comparative Analysis of Nucleotide Fluorescent Analogs for Registration of DNA Conformational Changes Induced by Interaction with Formamidopyrimidine-DNA Glycosylase Fpg. *Russ. J. Bioorg. Chem.* **2019**, *45*, 591–598. [CrossRef]
50. Kladova, O.A.; Kuznetsova, A.A.; Barthes, N.P.F.; Michel, B.Y.; Burger, A.; Fedorova, O.S.; Kuznetsov, N.A. New Fluorescent Analogs of Nucleotides Based on 3-Hydroxychromone for Recording Conformational Changes of DNA. *Russ. J. Bioorg. Chem.* **2019**, *45*, 598–606. [CrossRef]
51. Hopkins, B.B.; Reich, N.O. Simultaneous DNA Binding, Bending, and Base Flipping Evidence for a Novel M.EcoRI Methyltransferase-DNA Complex. *J. Biol. Chem.* **2004**, *279*, 37049–37060. [CrossRef] [PubMed]
52. Koval, V.V.; Kuznetsov, N.A.; Ishchenko, A.A.; Saparbaev, M.K.; Fedorova, O.S. Real-Time Studies of Conformational Dynamics of the Repair Enzyme E. Coli Formamidopyrimidine-DNA Glycosylase and Its DNA Complexes during Catalytic Cycle. *Mutat. Res.* **2010**, *685*, 3–10. [CrossRef]
53. Kuznetsov, N.A.; Koval, V.V.; Fedorova, O.S. Mechanism of Recognition and Repair of Damaged DNA by Human 8-Oxoguanine DNA Glycosylase HOGG1. *Biochemistry* **2011**, *76*, 118–130. [CrossRef] [PubMed]
54. Davletgildeeva, A.T.; Ishchenko, A.A.; Saparbaev, M.; Fedorova, O.S.; Kuznetsov, N.A. The Enigma of Substrate Recognition and Catalytic Efficiency of APE1-Like Enzymes. *Front. Cell Dev. Biol.* **2021**, *9*, 617161. [CrossRef] [PubMed]
55. Bakman, A.S.; Kuznetsova, A.A.; Yanshole, L.V.; Ishchenko, A.A.; Saparbaev, M.; Fedorova, O.S.; Kuznetsov, N.A. Fluorescently Labeled Human Apurinic/Apyrimidinic Endonuclease APE1 Reveals Effects of DNA Polymerase β on the APE1–DNA Interaction. *DNA Repair* **2023**, *123*, 103450. [CrossRef] [PubMed]
56. Kuznetsova, A.A.; Matveeva, A.G.; Milov, A.D.; Vorobjev, Y.N.; Dzuba, S.A.; Fedorova, O.S.; Kuznetsov, N.A. Substrate Specificity of Human Apurinic/Apyrimidinic Endonuclease APE1 in the Nucleotide Incision Repair Pathway. *Nucleic Acids Res.* **2018**, *46*, 11454–11465. [CrossRef]
57. Nevinsky, G.A. Structural, Thermodynamic, and Kinetic Basis for the Activities of Some Nucleic Acid Repair Enzymes. *J. Mol. Recognit.* **2011**, *24*, 656–677. [CrossRef]
58. David, S.S.; Williams, S.D. Chemistry of Glycosylases and Endonucleases Involved in Base-Excision Repair. *Chem. Rev.* **1998**, *98*, 1221–1261. [CrossRef]
59. Bjoras, M.; Luna, L.; Johnsen, B.; Hoff, E.; Haug, T.; Rognes, T.; Seeberg, E. Opposite Base-Dependent Reactions of a Human Base Excision Repair Enzyme on DNA Containing 7,8-Dihydro-8-Oxoguanine and Abasic Sites. *EMBO J.* **1997**, *16*, 6314–6322. [CrossRef] [PubMed]
60. Kuznetsov, N.A.; Koval, V.V.; Nevinsky, G.A.; Douglas, K.T.; Zharkov, D.O.; Fedorova, O.S. Kinetic Conformational Analysis of Human 8-Oxoguanine-DNA Glycosylase. *J. Biol. Chem.* **2007**, *282*, 1029–1038. [CrossRef] [PubMed]
61. Roldán-Arjona, T.; Wei, Y.F.; Carter, K.C.; Klungland, A.; Anselmino, C.; Wang, R.P.; Augustus, M.; Lindahl, T. Molecular Cloning and Functional Expression of a Human CDNA Encoding the Antimutator Enzyme 8-Hydroxyguanine-DNA Glycosylase. *Proc. Natl. Acad. Sci. USA* **1997**, *94*, 8016–8020. [CrossRef]
62. Radicella, J.P.P.; Dherin, C.; Desmaze, C.; Fox, M.S.S.; Boiteux, S. Cloning and Characterization of HOGG1, a Human Homolog of the OGG1 Gene of Saccharomyces Cerevisiae. *Proc. Natl. Acad. Sci. USA* **1997**, *94*, 8010–8015. [CrossRef]
63. Girard, P.M.; Guibourt, N.; Boiteux, S. The Ogg1 Protein of Saccharomyces Cerevisiae: A 7,8-Dihydro-8-Oxoguanine DNA Glycosylase/AP Lyase Whose Lysine 241 Is a Critical Residue for Catalytic Activity. *Nucleic Acids Res.* **1997**, *25*, 3404–3411. [CrossRef]
64. Kuznetsov, N.A.; Koval, V.V.; Zharkov, D.O.; Nevinsky, G.A.; Douglas, K.T.; Fedorova, O.S. Kinetics of Substrate Recognition and Cleavage by Human 8-Oxoguanine-DNA Glycosylase. *Nucleic Acids Res.* **2005**, *33*, 3919–3931. [CrossRef] [PubMed]
65. Zharkov, D.O.; Rosenquist, T.A.; Gerchman, S.E.; Grollman, A.P. Substrate Specificity and Reaction Mechanism of Murine 8-Oxoguanine-DNA Glycosylase. *J. Biol. Chem.* **2000**, *275*, 28607–28617. [CrossRef]
66. Bruner, S.D.D.; Norman, D.P.G.P.; Verdine, G.L.L. Structural Basis for Recognition and Repair of the Endogenous Mutagen 8-Oxoguanine in DNA. *Nature* **2000**, *403*, 859–866. [CrossRef]

67. Crenshaw, C.M.; Nam, K.; Oo, K.; Kutchukian, P.S.; Bowman, B.R.; Karplus, M.; Verdine, G.L. Enforced Presentation of an Extrahelical Guanine to the Lesion Recognition Pocket of Human 8-Oxoguanine Glycosylase, HOGG1. *J. Biol. Chem.* **2012**, *287*, 24916–24928. [CrossRef]
68. Kuznetsova, A.A.; Kuznetsov, N.A.; Ishchenko, A.A.; Saparbaev, M.K.; Fedorova, O.S. Step-by-Step Mechanism of DNA Damage Recognition by Human 8-Oxoguanine DNA Glycosylase. *Biochim. Biophys. Acta* **2014**, *1840*, 387–395. [CrossRef] [PubMed]
69. Lukina, M.V.; Kuznetsova, A.A.; Kuznetsov, N.A.; Fedorova, O.S. The Kinetic Analysis of Recognition of the Damaged Nucleotides by Mutant Forms of the 8-Oxoguanine DNA Glycosylase HOGG1. *Russ. J. Bioorg. Chem.* **2017**, *43*, 1–12. [CrossRef]
70. Tyugashev, T.E.; Vorobjev, Y.N.; Kuznetsova, A.A.; Lukina, M.V.; Kuznetsov, N.A.; Fedorova, O.S. Roles of Active-Site Amino Acid Residues in Specific Recognition of DNA Lesions by Human 8-Oxoguanine-DNA Glycosylase (OGG1). *J. Phys. Chem. B* **2019**, *123*, 4878–4887. [CrossRef] [PubMed]
71. Kuznetsova, A.A.; Kuznetsov, N.A.; Ishchenko, A.A.; Saparbaev, M.K.; Fedorova, O.S. Pre-Steady-State Fluorescence Analysis of Damaged DNA Transfer from Human DNA Glycosylases to AP Endonuclease APE1. *Biochim. Biophys. Acta* **2014**, *1840*, 3042–3051. [CrossRef] [PubMed]
72. Kuznetsov, N.A.; Kuznetsova, A.A.; Vorobjev, Y.N.; Krasnoperov, L.N.; Fedorova, O.S. Thermodynamics of the DNA Damage Repair Steps of Human 8-Oxoguanine DNA Glycosylase. *PLoS ONE* **2014**, *9*, e98495. [CrossRef]
73. Brooks, S.C.; Adhikary, S.; Rubinson, E.H.; Eichman, B.F. Recent Advances in the Structural Mechanisms of DNA Glycosylases. *Biochim. Biophys. Acta* **2013**, *1834*, 247–271. [CrossRef] [PubMed]
74. Au, K.G.; Cabrera, M.; Miller, J.H.; Modrich, P. Escherichia-Coli Muty Gene-Product Is Required for Specific a-G-]C.G Mismatch Correction. *Proc. Natl. Acad. Sci. USA* **1988**, *85*, 9163–9166. [CrossRef] [PubMed]
75. Lu, A.-L.; Tsai-Wu, J.-J.; Cillo, J. DNA Determinants and Substrate Specificities of *Escherichia coli* MutY. *J. Biol. Chem.* **1995**, *270*, 23582–23588. [CrossRef]
76. Bulychev, N.V.; Varaprasad, C.V.; Dorman, G.; Miller, J.H.; Eisenberg, M.; Grollman, A.P.; Johnson, F. Substrate Specificity of *Escherichia coli* MutY Protein. *Biochemistry* **1996**, *35*, 13147–13156. [CrossRef] [PubMed]
77. Tyugashev, T.E.; Kuznetsova, A.A.; Kuznetsov, N.A.; Fedorova, O.S. Interaction Features of Adenine DNA Glycosylase MutY from *E. coli* with DNA Substrates. *Russ. J. Bioorg. Chem.* **2017**, *43*, 13–22. [CrossRef]
78. Kuznetsov, N.A.; Kiryutin, A.S.; Kuznetsova, A.A.; Panov, M.S.; Barsukova, M.O.; Yurkovskaya, A.V.; Fedorova, O.S. The Formation of Catalytically Competent Enzyme-Substrate Complex Is Not a Bottleneck in Lesion Excision by Human Alkyladenine DNA Glycosylase. *J. Biomol. Struct. Dyn.* **2017**, *35*, 950–967. [CrossRef]
79. Petronzelli, F.; Riccio, A.; Markham, G.D.; Seeholzer, S.H.; Genuardi, M.; Karbowski, M.; Yeung, A.T.; Matsumoto, Y.; Bellacosa, A. Investigation of the Substrate Spectrum of the Human Mismatch-Specific DNA N-Glycosylase MED1 (MBD4): Fundamental Role of the Catalytic Domain. *J. Cell. Physiol.* **2000**, *185*, 473–480. [CrossRef]
80. Cortellino, S.; Turner, D.; Masciullo, V.; Schepis, F.; Albino, D.; Daniel, R.; Skalka, A.M.; Meropol, N.J.; Alberti, C.; Larue, L.; et al. The Base Excision Repair Enzyme MED1 Mediates DNA Damage Response to Antitumor Drugs and Is Associated with Mismatch Repair System Integrity. *Proc. Natl. Acad. Sci. USA* **2003**, *100*, 15071–15076. [CrossRef]
81. Yakovlev, D.A.; Kuznetsova, A.A.; Fedorova, O.S.; Kuznetsov, N.A. Search for Modified DNA Sites with the Human Methyl-CpG-Binding Enzyme MBD4. *Acta Nat.* **2017**, *9*, 88–98. [CrossRef]
82. Denver, D.R.; Swenson, S.L.; Lynch, M. An Evolutionary Analysis of the Helix-Hairpin-Helix Superfamily of DNA Repair Glycosylases. *Mol. Biol. Evol.* **2003**, *20*, 1603–1611. [CrossRef]
83. Kladova, O.A.; Krasnoperov, L.N.; Kuznetsov, N.A.; Fedorova, O.S. Kinetics and Thermodynamics of DNA Processing by Wild Type DNA-Glycosylase Endo III and Its Catalytically Inactive Mutant Forms. *Genes* **2018**, *9*, 190. [CrossRef] [PubMed]
84. Thayer, M.M.; Ahern, H.; Xing, D.; Cunningham, R.P.; Tainer, J.A. Novel DNA Binding Motifs in the DNA Repair Enzyme Endonuclease III Crystal Structure. *EMBO J.* **1995**, *14*, 4108–4120. [CrossRef]
85. Fromme, J.C.; Verdine, G.L. Structure of a Trapped Endonuclease III-DNA Covalent Intermediate. *EMBO J.* **2003**, *22*, 3461–3471. [CrossRef] [PubMed]
86. Kuznetsov, N.A.; Fedorova, O.S. Kinetic Milestones of Damage Recognition by DNA Glycosylases of the Helix-Hairpin-Helix Structural Superfamily. *Adv. Exp. Biol. Med.* **2020**, *1241*, 1–18.
87. Wallace, S.S.; Bandaru, V.; Kathe, S.D.; Bond, J.P. The Enigma of Endonuclease VIII. *DNA Repair* **2003**, *2*, 441–453. [CrossRef]
88. Jiang, D.; Hatahet, Z.; Melamede, R.J.; Kow, Y.W.; Wallace, S.S. Characterization of *Escherichia coli* Endonuclease VIII. *J. Biol. Chem.* **1997**, *272*, 32230–32239. [CrossRef]
89. Zharkov, D.O.; Golan, G.; Gilboa, R.; Fernandes, A.S.; Gerchman, S.E.; Kycia, J.H.; Rieger, R.A.; Grollman, A.P.; Shoham, G. Structural Analysis of an *Escherichia coli* Endonuclease VIII Covalent Reaction Intermediate. *EMBO J.* **2002**, *21*, 789–800. [CrossRef]
90. Zharkov, D.O.; Shoham, G.; Grollman, A.P. Structural Characterization of the Fpg Family of DNA Glycosylases. *DNA Repair* **2003**, *2*, 839–862. [CrossRef]
91. Kuznetsov, N.A.; Koval, V.V.; Zharkov, D.O.; Fedorova, O.S. Conformational Dynamics of the Interaction of *Escherichia coli* Endonuclease VIII with DNA Substrates. *DNA Repair* **2012**, *11*, 884–891. [CrossRef]
92. Kladova, O.A.; Kuznetsov, N.A.; Fedorova, O.S. Thermodynamic Parameters of Endonuclease VIII Interactions with Damaged DNA. *Acta Nat.* **2019**, *11*, 29–37. [CrossRef]
93. Kladova, O.A.; Kuznetsova, A.A.; Fedorova, O.S.; Kuznetsov, N.A. Mutational and Kinetic Analysis of Lesion Recognition by *Escherichia coli* Endonuclease VIII. *Genes* **2017**, *8*, 140. [CrossRef]

94. Tchou, J.; Kasai, H.; Shibutani, S.; Chung, M.H.; Laval, J.; Grollman, A.P.; Nishimura, S. 8-Oxoguanine (8-Hydroxyguanine) DNA Glycosylase and Its Substrate Specificity. *Proc. Natl. Acad. Sci. USA* **1991**, *88*, 4690–4694. [CrossRef] [PubMed]
95. Chung, M.H.; Kasai, H.; Jones, D.S.; Inoue, H.; Ishikawa, H.; Ohtsuka, E.; Nishimura, S. An Endonuclease Activity of *Escherichia-coli* That Specifically Removes 8-Hydroxyguanine Residues from DNA. *Mutat. Res.* **1991**, *254*, 1–12. [CrossRef]
96. Gilboa, R.; Zharkov, D.O.; Golan, G.; Fernandes, A.S.; Gerchman, S.E.; Matz, E.; Kycia, J.H.; Grollman, A.P.; Shoham, G. Structure of Formamidopyrimidine-DNA Glycosylase Covalently Complexed to DNA. *J. Biol. Chem.* **2002**, *277*, 19811–19816. [CrossRef]
97. Kuznetsov, N.A.; Zharkov, D.O.; Koval, V.V.; Buckle, M.; Fedorova, O.S. Reversible Chemical Step and Rate-Limiting Enzyme Regeneration in the Reaction Catalyzed by Formamidopyrimidine-DNA Glycosylase. *Biochemistry* **2009**, *48*, 11335–11343. [CrossRef] [PubMed]
98. Kuznetsov, N.A.; Milov, A.D.; Koval, V.V.; Samoilova, R.I.; Grishin, Y.A.; Knorre, D.G.; Tsvetkov, Y.D.; Fedorova, O.S.; Dzuba, S.A. PELDOR Study of Conformations of Double-Spin-Labeled Single- and Double-Stranded DNA with Non-Nucleotide Inserts. *Phys. Chem. Chem. Phys.* **2009**, *11*, 6826–6832. [CrossRef] [PubMed]
99. Kuznetsov, N.A.; Milov, A.D.; Isaev, N.P.; Vorobjev, Y.N.; Koval, V.V.; Dzuba, S.A.; Fedorova, O.S.; Tsvetkov, Y.D. PELDOR Analysis of Enzyme-Induced Structural Changes in Damaged DNA Duplexes. *Mol. Biosyst.* **2011**, *7*, 2670–2680. [CrossRef] [PubMed]
100. Prakash, A.; Doublie, S.; Wallace, S.S. The Fpg/Nei Family of DNA Glycosylases: Substrates, Structures, and Search for Damage. *Prog. Mol. Biol. Transl. Sci.* **2012**, *110*, 71–91. [CrossRef]
101. Hazra, T.K.; Mitra, S. Purification and Characterization of NEIL1 and NEIL2, Members of a Distinct Family of Mammalian DNA Glycosylases for Repair of Oxidized Bases. *DNA Repair Pt. A* **2006**, *408*, 33–48. [CrossRef]
102. Doublie, S.; Bandaru, V.; Bond, J.P.; Wallace, S.S. The Crystal Structure of Human Endonuclease VIII-like 1 (NEIL1) Reveals a Zincless Finger Motif Required for Glycosylase Activity. *Proc. Natl. Acad. Sci. USA* **2004**, *101*, 10284–10289. [CrossRef]
103. Prakash, A.; Carroll, B.L.; Sweasy, J.B.; Wallace, S.S.; Doublie, S. Genome and Cancer Single Nucleotide Polymorphisms of the Human NEIL1 DNA Glycosylase: Activity, Structure, and the Effect of Editing. *DNA Repair* **2014**, *14*, 17–26. [CrossRef]
104. Kladova, O.A.; Grin, I.R.; Fedorova, O.S.; Kuznetsov, N.A.; Zharkov, D.O. Conformational Dynamics of Damage Processing by Human DNA Glycosylase NEIL1. *J. Mol. Biol.* **2019**, *431*, 1098–1112. [CrossRef] [PubMed]
105. Demple, B.; Sung, J.-S. Molecular and Biological Roles of Ape1 Protein in Mammalian Base Excision Repair. *DNA Repair* **2005**, *4*, 1442–1449. [CrossRef]
106. Gros, L.; Ishchenko, A.A.; Ide, H.; Elder, R.H.; Saparbaev, M.K. The Major Human AP Endonuclease (Ape1) Is Involved in the Nucleotide Incision Repair Pathway. *Nucleic Acids Res.* **2004**, *32*, 73–81. [CrossRef] [PubMed]
107. Li, M.; Wilson, D.M., 3rd. Human Apurinic/Apyrimidinic Endonuclease 1. *Antioxid. Redox Signal* **2014**, *20*, 678–707. [CrossRef]
108. Dodson, M.L.; Lloyd, R.S. Mechanistic Comparison among Base Exision Repair Glycosylases. *Free Radic. Biol. Med.* **2002**, *32*, 678–682. [CrossRef] [PubMed]
109. Burrows, C.J.; Muller, J.G. Oxidative Nucleobase Modifications Leading to Strand Scission. *Chem. Rev.* **1998**, *98*, 1109–1152. [CrossRef] [PubMed]
110. Jacobs, A.L.; Schar, P. DNA Glycosylases: In DNA Repair and Beyond. *Chromosoma* **2012**, *121*, 1–20. [CrossRef]
111. Boiteux, S.; Guillet, M. Abasic Sites in DNA: Repair and Biological Consequences in Saccharomyces Cerevisiae. *DNA Repair* **2004**, *3*, 1–12. [CrossRef]
112. Chen, D.S.; Herman, T.; Demple, B. Two Distinct Human DNA Diesterases That Hydrolyze 3′-Blocking Deoxyribose Fragments from Oxidized DNA. *Nucleic Acids Res.* **1991**, *19*, 5907–5914. [CrossRef]
113. Golan, G.; Ishchenko, A.A.; Khassenov, B.; Shoham, G.; Saparbaev, M.K. Coupling of the Nucleotide Incision and 3′-5′ Exonuclease Activities in *Escherichia coli* Endonuclease IV: Structural and Genetic Evidences. *Mutat. Res.* **2010**, *685*, 70–79. [CrossRef] [PubMed]
114. Prorok, P.; Saint-Pierre, C.; Gasparutto, D.; Fedorova, O.S.; Ishchenko, A.A.; Leh, H.; Buckle, M.; Tudek, B.; Saparbaev, M. Highly Mutagenic Exocyclic DNA Adducts Are Substrates for the Human Nucleotide Incision Repair Pathway. *PLoS ONE* **2012**, *7*, e51776. [CrossRef] [PubMed]
115. Christov, P.P.; Banerjee, S.; Stone, M.P.; Rizzo, C.J. Selective Incision of the Alpha-N-Methyl-Formamidopyrimidine Anomer by *Escherichia coli* Endonuclease IV. *J. Nucleic Acids* **2010**, *2010*, 850234. [CrossRef] [PubMed]
116. Vrouwe, M.G.; Pines, A.; Overmeer, R.M.; Hanada, K.; Mullenders, L.H. UV-Induced Photolesions Elicit ATR-Kinase-Dependent Signaling in Non-Cycling Cells through Nucleotide Excision Repair-Dependent and -Independent Pathways. *J. Cell Sci.* **2011**, *124*, 435–446. [CrossRef]
117. Guliaev, A.B.; Hang, B.; Singer, B. Structural Insights by Molecular Dynamics Simulations into Specificity of the Major Human AP Endonuclease toward the Benzene-Derived DNA Adduct, PBQ-C. *Nucleic Acids Res.* **2004**, *32*, 2844–2852. [CrossRef]
118. Daviet, S.; Couve-Privat, S.; Gros, L.; Shinozuka, K.; Ide, H.; Saparbaev, M.; Ishchenko, A.A. Major Oxidative Products of Cytosine Are Substrates for the Nucleotide Incision Repair Pathway. *DNA Repair* **2007**, *6*, 8–18. [CrossRef]
119. Prorok, P.; Alili, D.; Saint-Pierre, C.; Gasparutto, D.; Zharkov, D.O.; Ishchenko, A.A.; Tudek, B.; Saparbaev, M.K. Uracil in Duplex DNA Is a Substrate for the Nucleotide Incision Repair Pathway in Human Cells. *Proc. Natl. Acad. Sci. USA* **2013**, *110*, E3695–E3703. [CrossRef]
120. Barzilay, G.; Walker, L.J.; Robson, C.N.; Hickson, I.D. Site-Directed Mutagenesis of the Human DNA Repair Enzyme HAP1: Identification of Residues Important for AP Endonuclease and RNase H Activity. *Nucleic Acids Res.* **1995**, *23*, 1544–1550. [CrossRef]

121. Berquist, B.R.; McNeill, D.R.; Wilson, D.M., 3rd. Characterization of Abasic Endonuclease Activity of Human Ape1 on Alternative Substrates, as Well as Effects of ATP and Sequence Context on AP Site Incision. *J. Mol. Biol.* **2008**, *379*, 17–27. [CrossRef]
122. Barnes, T.; Kim, W.C.; Mantha, A.K.; Kim, S.E.; Izumi, T.; Mitra, S.; Lee, C.H. Identification of Apurinic/Apyrimidinic Endonuclease 1 (APE1) as the Endoribonuclease That Cleaves c-Myc MRNA. *Nucleic Acids Res.* **2009**, *37*, 3946–3958. [CrossRef]
123. Chou, K.M.; Cheng, Y.C. An Exonucleolytic Activity of Human Apurinic/Apyrimidinic Endonuclease on 3′ Mispaired DNA. *Nature* **2002**, *415*, 655–659. [CrossRef]
124. Kerins, S.M.; Collins, R.; McCarthy, T.V. Characterization of an Endonuclease IV 3′-5′ Exonuclease Activity. *J. Biol. Chem.* **2003**, *278*, 3048–3054. [CrossRef]
125. Schormann, N.; Ricciardi, R.; Chattopadhyay, D. Uracil-DNA Glycosylases-Structural and Functional Perspectives on an Essential Family of DNA Repair Enzymes. *Protein Sci.* **2014**, *23*, 1667–1685. [CrossRef] [PubMed]
126. Huffman, J.L.; Sundheim, O.; Tainer, J.A. DNA Base Damage Recognition and Removal: New Twists and Grooves. *Mutat. Res.* **2005**, *577*, 55–76. [CrossRef] [PubMed]
127. Mullins, E.A.; Shi, R.X.; Parsons, Z.D.; Yuen, P.K.; David, S.S.; Igarashi, Y.; Eichman, B.F. The DNA Glycosylase AlkD Uses a Non-Base-Flipping Mechanism to Excise Bulky Lesions. *Nature* **2015**, *527*, 254–258. [CrossRef] [PubMed]
128. Dunn, A.R.; Kad, N.M.; Nelson, S.R.; Warshaw, D.M.; Wallace, S.S. Single Qdot-Labeled Glycosylase Molecules Use a Wedge Amino Acid to Probe for Lesions While Scanning along DNA. *Nucleic Acids Res.* **2011**, *39*, 7487–7498. [CrossRef]
129. Kuznetsova, A.A.; Iakovlev, D.A.; Misovets, I.V.; Ishchenko, A.A.; Saparbaev, M.K.; Kuznetsov, N.A.; Fedorova, O.S. Pre-Steady-State Kinetic Analysis of Damage Recognition by Human Single-Strand Selective Monofunctional Uracil-DNA Glycosylase SMUG1. *Mol. Biosyst.* **2017**, *13*, 2638–2649. [CrossRef]
130. Nelson, S.R.; Dunn, A.R.; Kathe, S.D.; Warshaw, D.M.; Wallace, S.S. Two Glycosylase Families Diffusively Scan DNA Using a Wedge Residue to Probe for and Identify Oxidatively Damaged Bases. *Proc. Natl. Acad. Sci. USA* **2014**, *111*, E2091-9. [CrossRef]
131. Kuznetsov, N.A.; Bergonzo, C.; Campbell, A.J.; Li, H.; Mechetin, G.V.; de los Santos, C.; Grollman, A.P.; Fedorova, O.S.; Zharkov, D.O.; Simmerling, C. Active Destabilization of Base Pairs by a DNA Glycosylase Wedge Initiates Damage Recognition. *Nucleic Acids Res.* **2015**, *43*, 272–281. [CrossRef]
132. Lee, A.J.; Wallace, S.S. Hide and Seek: How Do DNA Glycosylases Locate Oxidatively Damaged DNA Bases amidst a Sea of Undamaged Bases? *Free Radic. Biol. Med.* **2017**, *107*, 170–178. [CrossRef]
133. Mol, C.D.; Hosfield, D.J.; Tainer, J.A. Abasic Site Recognition by Two Apurinic/Apyrimidinic Endonuclease Families in DNA Base Excision Repair: The 3′ Ends Justify the Means. *Mutat. Res.* **2000**, *460*, 211–229. [CrossRef]
134. Tsutakawa, S.E.; Shin, D.S.; Mol, C.D.; Izumi, T.; Arvai, A.S.; Mantha, A.K.; Szczesny, B.; Ivanov, I.N.; Hosfield, D.J.; Maiti, B.; et al. Conserved Structural Chemistry for Incision Activity in Structurally Non-Homologous Apurinic/Apyrimidinic Endonuclease APE1 and Endonuclease IV DNA Repair Enzymes. *J. Biol. Chem.* **2013**, *288*, 8445–8455. [CrossRef] [PubMed]
135. Beernink, P.T.; Segelke, B.W.; Hadi, M.Z.; Erzberger, J.P.; Wilson, D.M., 3rd; Rupp, B. Two Divalent Metal Ions in the Active Site of a New Crystal Form of Human Apurinic/Apyrimidinic Endonuclease, Ape1: Implications for the Catalytic Mechanism. *J. Mol. Biol.* **2001**, *307*, 1023–1034. [CrossRef]
136. Gorman, M.A.; Morera, S.; Rothwell, D.G.; de La Fortelle, E.; Mol, C.D.; Tainer, J.A.; Hickson, I.D.; Freemont, P.S. The Crystal Structure of the Human DNA Repair Endonuclease HAP1 Suggests the Recognition of Extra-Helical Deoxyribose at DNA Abasic Sites. *EMBO J.* **1997**, *16*, 6548–6558. [CrossRef] [PubMed]
137. Manvilla, B.A.; Pozharski, E.; Toth, E.A.; Drohat, A.C. Structure of Human Apurinic/Apyrimidinic Endonuclease 1 with the Essential Mg^{2+} Cofactor. *Acta Crystallogr. D Biol. Crystallogr.* **2013**, *69*, 2555–2562. [CrossRef]
138. Mol, C.D.; Izumi, T.; Mitra, S.; Tainer, J.A. DNA-Bound Structures and Mutants Reveal Abasic DNA Binding by APE1 and DNA Repair Coordination. *Nature* **2000**, *403*, 451–456. [CrossRef]
139. Timofeyeva, N.A.; Koval, V.V.; Knorre, D.G.; Zharkov, D.O.; Saparbaev, M.K.; Ishchenko, A.A.; Fedorova, O.S. Conformational Dynamics of Human AP Endonuclease in Base Excision and Nucleotide Incision Repair Pathways. *J. Biomol. Struct. Dyn.* **2009**, *26*, 637–652. [CrossRef]
140. Kanazhevskaya, L.Y.; Koval, V.V.; Zharkov, D.O.; Strauss, P.R.; Fedorova, O.S. Conformational Transitions in Human AP Endonuclease 1 and Its Active Site Mutant during Abasic Site Repair. *Biochemistry* **2010**, *49*, 6451–6461. [CrossRef]
141. Kanazhevskaya, L.Y.; Koval, V.V.; Vorobjev, Y.N.; Fedorova, O.S. Conformational Dynamics of Abasic DNA upon Interactions with AP Endonuclease 1 Revealed by Stopped-Flow Fluorescence Analysis. *Biochemistry* **2012**, *51*, 1306–1321. [CrossRef]
142. Bulygin, A.A.; Syryamina, V.N.; Kuznetsova, A.A.; Novopashina, D.S.; Dzuba, S.A.; Kuznetsov, N.A. Inner Amino Acid Contacts Are Key Factors of Multistage Structural Rearrangements of DNA and Affect Substrate Specificity of Apurinic/Apyrimidinic Endonuclease APE1. *Int. J. Mol. Sci.* **2023**, *24*, 11474. [CrossRef] [PubMed]
143. Senchurova, S.I.; Syryamina, V.N.; Kuznetsova, A.A.; Novopashina, D.S.; Ishchenko, A.A.; Saparbaev, M.; Dzuba, S.A.; Fedorova, O.S.; Kuznetsov, N.A. The Mechanism of Damage Recognition by Apurinic/Apyrimidinic Endonuclease Nfo from *Escherichia coli*. *BBA—Gen. Subj.* **2022**, *1866*, 130216. [CrossRef] [PubMed]
144. Bulygin, A.A.; Fedorova, O.S.; Kuznetsov, N. Insights into Mechanisms of Damage Recognition and Catalysis by APE1-like Enzymes. *Int. J. Mol. Sci.* **2022**, *23*, 4361. [CrossRef] [PubMed]
145. Bulygin, A.A.; Kuznetsova, A.A.; Vorobjev, Y.N.; Fedorova, O.S.; Kuznetsov, N.A. The Role of Active-Site Plasticity in Damaged-Nucleotide Recognition by Human Apurinic/Apyrimidinic Endonuclease APE1. *Molecules* **2020**, *25*, 3940. [CrossRef] [PubMed]

146. Alekseeva, I.V.; Kuznetsova, A.A.; Bakman, A.S.; Fedorova, O.S.; Kuznetsov, N.A. The Role of Active-Site Amino Acid Residues in the Cleavage of DNA and RNA Substrates by Human Apurinic/Apyrimidinic Endonuclease APE1. *BBA—Gen. Subj.* **2020**, *1864*, 129718. [CrossRef] [PubMed]
147. Alekseeva, I.V.; Bakman, A.S.; Vorobjev, Y.N.; Fedorova, O.S.; Kuznetsov, N.A. Role of Ionizing Amino Acid Residues in the Process of DNA Binding by Human AP Endonuclease 1 and in Its Catalysis. *J. Phys. Chem. B* **2019**, *123*, 9546–9556. [CrossRef]
148. Alekseeva, I.V.; Davletgildeeva, A.T.; Arkova, O.V.; Kuznetsov, N.A.; Fedorova, O.S. The Impact of Single-Nucleotide Polymorphisms of Human Apurinic/Apyrimidinic Endonuclease 1 on Specific DNA Binding and Catalysis. *Biochimie* **2019**, *163*, 73–83. [CrossRef]
149. Bakman, A.S.; Boichenko, S.S.; Kuznetsova, A.A.; Ishchenko, A.A.; Saparbaev, M.; Kuznetsov, N.A. The Impact of Human DNA Glycosylases on the Activity of DNA Polymerase β toward Various Base Excision Repair Intermediates. *Int. J. Mol. Sci.* **2023**, *24*, 9594. [CrossRef]
150. Davletgildeeva, A.T.; Kuznetsova, A.A.; Novopashina, D.S.; Ishchenko, A.A.; Saparbaev, M.; Fedorova, O.S.; Kuznetsov, N.A. Comparative Analysis of Exo-and Endonuclease Activities of APE1-like Enzymes. *Int. J. Mol. Sci.* **2022**, *23*, 2869. [CrossRef]
151. Kuznetsova, A.A.; Gavrilova, A.A.; Novopashina, D.S.; Fedorova, O.S.; Kuznetsov, N.A. Mutational and Kinetic Analysis of APE1 Endoribonuclease Activity. *Mol. Biol.* **2021**, *55*, 211–224. [CrossRef]
152. Miroshnikova, A.D.; Kuznetsova, A.A.; Vorobjev, Y.N.; Kuznetsov, N.A.; Fedorova, O.S. Effects of Mono- and Divalent Metal Ions on DNA Binding and Catalysis of Human Apurinic/Apyrimidinic Endonuclease 1. *Mol. BioSyst.* **2016**, *12*, 1527–1539. [CrossRef]
153. Miroshnikova, A.D.; Kuznetsova, A.A.; Kuznetsov, N.A.; Fedorova, O.S. Thermodynamics of Damaged DNA Binding and Catalysis by Human AP Endonuclease 1. *Acta Nat.* **2016**, *8*, 103–110. [CrossRef]